A covalently bound inhibitor triggers EZH2 degradation through CHIP#mediated ubiquitination

Article

SOURCE DATA | OPEN ACCESS

THE EMBO JOURNAL

A covalently bound inhibitor triggers EZH2 degradation through CHIP-mediated ubiquitination

Xu Wang[1,2], Wei Cao[1,2], Jianjun Zhang[1,2], Ming Yan[1,2], Qin Xu[1,2], Xiangbing Wu[1,2], Lixin Wan[3], Zhiyuan Zhang[1,2], Chenping Zhang[1,2], Xing Qin[1,2], Meng Xiao[1,2], Dongxia Ye[2], Yuyang Liu[2], Zeguang Han[4], Shaomeng Wang[5], Li Mao[1,6], Wenyi Wei[3,*] & Wantao Chen[1,2,**]

Abstract

Enhancer of zeste homolog 2 (EZH2) has been characterized as a critical oncogene and a promising drug target in human malignant tumors. The current EZH2 inhibitors strongly suppress the enhanced enzymatic function of mutant EZH2 in some lymphomas. However, the recent identification of a PRC2- and methyltransferase-independent role of EZH2 indicates that a complete suppression of all oncogenic functions of EZH2 is needed. Here, we report a unique EZH2-targeting strategy by identifying a gambogenic acid (GNA) derivative as a novel agent that specifically and covalently bound to Cys668 within the EZH2-SET domain, triggering EZH2 degradation through COOH terminus of Hsp70-interacting protein (CHIP)-mediated ubiquitination. This class of inhibitors significantly suppressed H3K27Me3 and effectively reactivated polycomb repressor complex 2 (PRC2)-silenced tumor suppressor genes. Moreover, the novel inhibitors significantly suppressed tumor growth in an EZH2-dependent manner, and tumors bearing a non-GNA-interacting C668S-EZH2 mutation exhibited resistance to the inhibitors. Together, our results identify the inhibition of the signaling pathway that governs GNA-mediated destruction of EZH2 as a promising anti-cancer strategy.

Keywords CHIP; covalent inhibitor; EZH2; oncoprotein; ubiquitination
Subject Categories Cancer; Chromatin, Epigenetics, Genomics & Functional Genomics; Post-translational Modifications, Proteolysis & Proteomics
DOI 10.15252/embj.201694058 | Received 6 February 2016 | Revised 28 September 2016 | Accepted 15 February 2017 | Published online 20 March 2017
The EMBO Journal (2017) 36: 1243–1260

Introduction

In eukaryotes, post-translational modifications of histones, such as methylation, acetylation, phosphorylation, and ubiquitination, are critical for regulating chromatin structure and gene expression (Cao *et al*, 2002; Plath *et al*, 2003). The methylation of lysine residues within the histone tails, a process that is promoted by methyltransferases and antagonized by the histone demethylases, has been characterized as a major regulatory step (Shangary *et al*, 2008). In this regard, the histone methyltransferase enhancer of zeste homolog 2 (EZH2) and its binding partners SUZ12 polycomb repressive complex 2 subunit (SUZ12) and embryonic ectoderm development (EED) form the multi-subunit polycomb repressor complex 2 (PRC2) to trimethylate histone H3 at the K27 (Bracken & Helin, 2009; Ezhkova *et al*, 2009; Shih *et al*, 2012) residue. Biologically, H3K27Me3 has been largely characterized to function as a suppressive marker of gene transcription (Cao *et al*, 2002). EZH2 has received increasing attention in recent years for its oncogenic roles in driving aggressive human cancers (Cao *et al*, 2011; Chang *et al*, 2011). Consistent with this notion, aberrant overexpression of EZH2 and gain-of-function EZH2 mutations has been frequently observed in various human malignancies (Jones & Baylin, 2007; Chang *et al*, 2011), and EZH2 overexpression could drive normal cells to de-differentiate, subsequently acquiring stem cell-like features (Sparmann & van Lohuizen, 2006; Jones & Baylin, 2007; Kondo *et al*, 2008; Cao *et al*, 2011). Mechanistically, previous studies have revealed that the oncogenic roles of EZH2 are largely due to its ability to suppress the expression of a cohort of downstream tumor suppressor targets via H3K27 trimethylation-mediated epigenetic silencing (Bonasio *et al*, 2010). To this end, most of the currently developed EZH2 inhibitors are designed to suppress the H3K27-trimethyltransferase enzymatic activity of EZH2 against lymphomas with mutant EZH2, which exhibits

1 Faculty of Oral and Maxillofacial Surgery, Department of Oral and Maxillofacial Head & Neck Oncology, Ninth People's Hospital, Shanghai Jiao Tong University School of Medicine, Shanghai, China
2 Shanghai Key Laboratory of Stomatology, Shanghai Research Institute of Stomatology, Shanghai, China
3 Department of Pathology, Beth Israel Deaconess Medical Center, Harvard Medical School, Boston, MA, USA
4 Shanghai Center for Systems Biomedicine, Shanghai Jiao Tong University, Shanghai, China
5 Comprehensive Cancer Center, Departments of Internal Medicine, Pharmacology and Medicinal Chemistry, University of Michigan, Ann Arbor, MI, USA
6 Department of Oncology and Diagnostic Sciences, University of Maryland School of Dentistry, Baltimore, MD, USA
*Corresponding author. Tel: +1 617 735 2495; E-mail: wwei2@bidmc.harvard.edu
**Corresponding author. Tel: +86 021 23271699 5211; E-mail: chenwantao196323@sjtu.edu.cn

enhanced enzymatic function (Knutson *et al*, 2012; McCabe *et al*, 2012; Qi *et al*, 2012; Xu *et al*, 2015).

However, recent findings have begun to reveal that EZH2 can also exert its oncogenic roles independent of PRC2 by switching from a polycomb repressor to a transcriptional co-activator independent of its intrinsic histone methyltransferase activity (Xu *et al*, 2012; Yan *et al*, 2013; Kim *et al*, 2015). Moreover, acquired resistance to EZH2 enzymatic inhibitor may arise in cancer patients in part through mutations in the EZH2 oncoprotein. Even though there is demonstrated potential for active site-inhibitor-resistant EZH2 mutants that remains targetable by the second-generation EZH2 enzymatic inhibitors (Baker *et al*, 2015; Gibaja *et al*, 2016), there is increasing needs to expand the arsenal of EZH2 targeting drugs, potentially with different functional mechanisms in further suppressing EZH2. To this end, the discovery of a PRC2-independent as well as a methyltransferase-independent mechanism for EZH2 in promoting tumorigenesis suggests that simply inhibiting the enzymatic activity of EZH2 methyltransferase cannot fully terminate its oncogenic functions (Xu *et al*, 2012). Therefore, there is a need for developing novel EZH2 inhibitors that are capable of decreasing the abundance of the EZH2 oncoprotein and that will serve as a novel anti-cancer therapy to reverse PRC2-mediated epigenetic gene silencing.

To develop such inhibitors, triggering the degradation of the EZH2 oncoprotein, rather than the simple inhibition of its enzymatic activity (Miranda *et al*, 2009; Kim *et al*, 2013b), will be a more effective strategy. To this end, given that the ubiquitin–proteasome pathway is a major system in mammal cells for controlling protein stability and fate, the stability of EZH2 is also controlled by the E3 ligases Smurf2 (Yu *et al*, 2013) and β-TrCP (Sahasrabuddhe *et al*, 2015). However, it remains largely undefined whether these two E3 ligases are mutated or inactivated to allow the aberrant elevation of EZH2 in human cancers, whether these two E3 ligases play physiological roles in triggering EZH2 degradation upon environmental challenges and whether the misregulation of this process contributes to the pathological role of EZH2 in driving malignancy.

Gambogenic acid is natural compound derived from gamboge and is reported as a potent anti-cancer agent for many types of human cancers (Yan *et al*, 2011; Yu *et al*, 2012). Its chemical structure contains active bond, which is able to bind with target protein, but the detailed molecular mechanism underlying its anti-cancer effects remains not fully understood. Here, we reported that gambogenic acid (GNA) derivatives function as a novel class of EZH2 inhibitor by direct and covalent binding of EZH2, a process that is sufficient to disassociate the PRC2 complex, thus inhibiting its methyltransferase activity. Moreover, we also demonstrated that covalently GNA-modified EZH2 could be targeted for ubiquitination-mediated degradation by the COOH terminus of Hsp70-interacting protein (CHIP), a key player in the protein quality control system that mediates the polyubiquitination of misfolded or aggregated proteins for degradation (Whitesell & Lindquist, 2005; Ferreira *et al*, 2013). Our studies therefore reveal a novel class of EZH2 inhibitors that could achieve superior anti-cancer effects by not only inhibiting EZH2 enzymatic activity but also promoting its ubiquitination-mediated degradation to fully inhibit its oncogenic functions.

Results

The Cys668 residue within the EZH2 SET domain covalently binds to gambogenic acid

To search for a novel EZH2 inhibitory mechanism, we focused on identifying agents that specifically decrease EZH2 expression. To achieve this goal, we screened a chemical library of 1215 chemical compounds with a high-content screening Operetta platform (PerkinElmer, Waltham, MA, USA) using human epithelial cancer HN-6 cells. These cells firmly adhere to the cell culture plate, thus allowing for clear imaging. After incubation with compounds for 24 h, the immunofluorescent signals of EZH2 were analyzed with the Harmony 3 software. Notably, GNA was the most effective of the 1215 compounds in reducing EZH2 immunofluorescent signals (Appendix Fig S1A and B). Consistent with this finding, we further found that GNA (Appendix Fig S1C) significantly reduced EZH2 nuclear abundance (Fig 1A). More importantly, in support of a direct interaction between GNA and EZH2 as a possible mechanism to suppress EZH2, we detected a co-localization of Bio-GNA with endogenous EZH2 in the nuclei of HN-6 cells using immunofluorescence analysis following a short-term (2-h) incubation (Fig 1B).

Subsequently, to search for GNA-interacting cellular proteins as possible direct-binding target(s), we performed affinity pull-down assays using Bio-GNA (Appendix Fig S1F) conjugated to streptavidin–agarose beads followed by high-performance liquid chromatography–tandem mass spectrometry (HPLC-MS/MS) analysis. Our analysis identified HSP90, tubulin, and EZH2 as the top hits of the GNA-interacting proteins (Appendix Table S1). Furthermore, the GNA-interacting 95-kD band was validated as the EZH2 protein (Appendix Fig S1G and H), indicating a possible direct binding between EZH2 and GNA. Consistent with this finding, we further demonstrated that GNA specifically interacted with EZH2 and other known PRC2 complex components, such as SUZ12 and EED (Fig 1C). On the other hand, unconjugated, free GNA could specifically compete with Bio-GNA to associate with endogenous EZH2 (Fig 1C). Strikingly, GNA did not interact with the EZH2 close homolog EZH1, or other examined SET domain containing methyltransferases, such as SET8 and ESET. These results demonstrate that the interaction between GNA and EZH2 was specific, at least in this experimental setting (Fig 1C).

Notably, we observed a time-dependent increase in the association between Bio-GNA and recombinant C-terminal EZH2 in denatured sodium dodecyl sulfate–polyacrylamide gel electrophoresis (SDS–PAGE) gels (Fig 1D), suggesting that a possible covalent bonding was involved in the interaction that is resistant to SDS-mediated denaturing experimental conditions (Zhou *et al*, 2009). A series of deletion experiments allowed us to further pinpoint the C-terminal SET domain within EZH2 as the major binding site for GNA (Appendix Fig S2A–C). Given the critical role of cysteine residues in mediating the characterized "Michael reaction" between a given agent and its direct targets (Yun *et al*, 2008), the contribution of the three cysteine residues within the EZH2-SET domain to its specific association with GNA was further explored. Interestingly, only mutating C668, but not the other two cysteine residues (C647 and C699), specifically abolished the interaction between EZH2 and GNA (Fig 2A and B). Interestingly, the GNA non-interacting EZH1

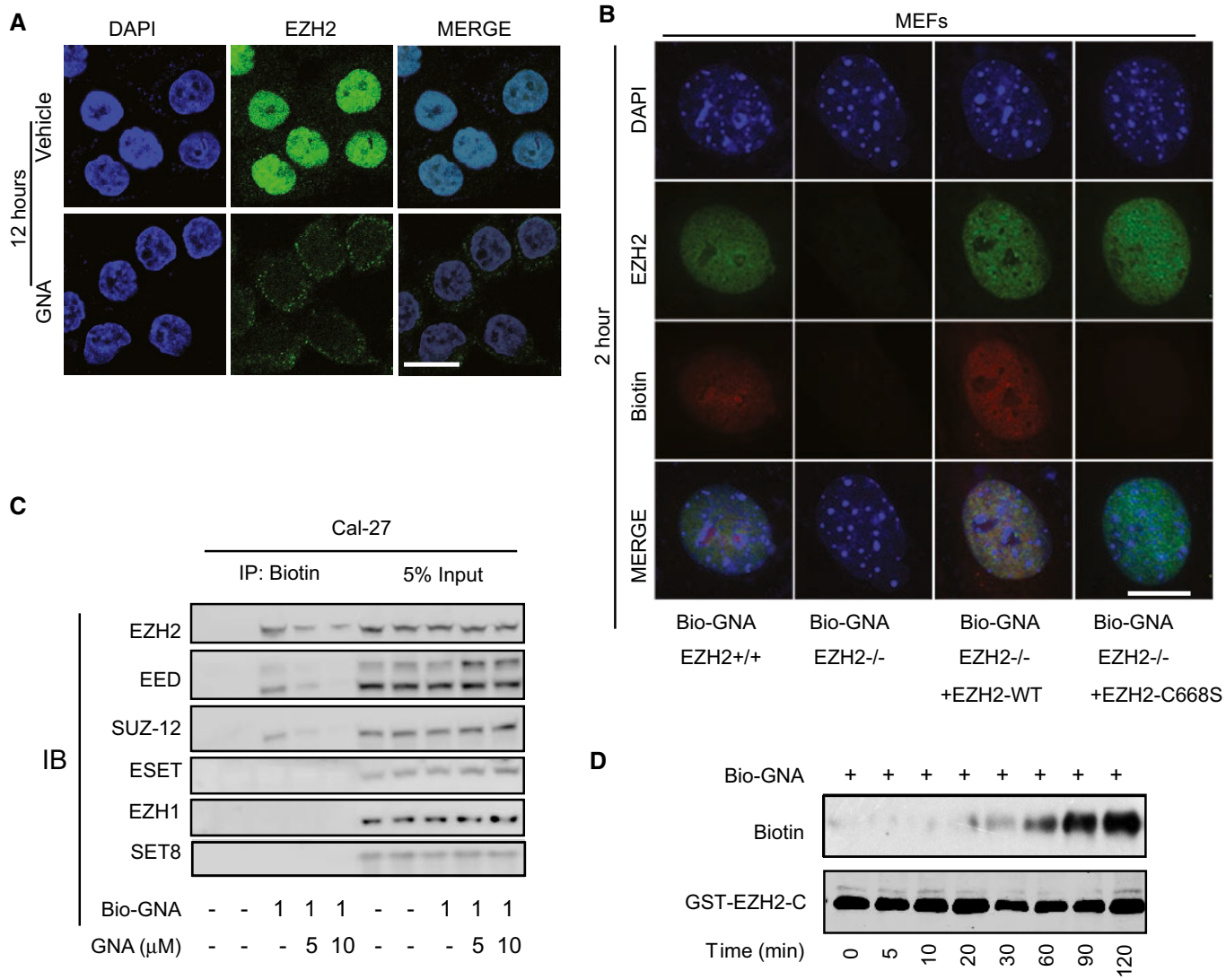

Figure 1. Screening and identification of gambogenic acid (GNA) to directly interact with EZH2.

A Immunofluorescence analysis demonstrated that a 12-h treatment with 2 μM GNA decreased the abundance of endogenous EZH2 in the nuclei of HN-6 head and neck cancer cells. Scale bar, 25 μm.

B Immunofluorescence analysis demonstrated that biotinylated GNA (Bio-GNA) co-localized with EZH2 in the nuclei of mouse embryonic fibroblasts (MEFs). Scale bar, 25 μm.

C *In vitro* binding assays coupled with immunoblot assays reveal that Bio-GNA bound to EZH2 in the whole-cell lysate derived from Cal-27 head and neck cancer cells, whereas free, unconjugated GNA efficiently competed with Bio-GNA to bind endogenous EZH2. After the cells were lysed to generate whole-cell lysates, the indicated concentration of Bio-GNA or free GNA was added to perform the *in vitro* binding assays.

D Bio-GNA (5 μM) binds to the recombinant C-terminal portion of EZH2 in a time-dependent manner.

Source data are available online for this figure.

has a serine residue (Ser664) in the EZH2-C668 corresponding position, while the S664C-EZH1 acquired ability to interact with GNA, in a similar fashion as EZH2 (Fig 2B). Given that EZH1 is highly homologous to EZH2, these results support the notion that the presence of the C668 residue in EZH2 but not in EZH1 confers the specificity for GNA and GNA derivative GNA002 to directly interact with EZH2 in a relatively specific fashion.

Similarly, computational modeling revealed a favorable covalent C-S bond with the Michael acceptor on the C8 atom of GNA bridging to the S atom of Cys668 within WT-EZH2 (Appendix Fig S2D–F). On the other hand, the EZH1-like, C668S mutant form of EZH2 does not contain an S atom as a receptor (Appendix Fig S2D–F) and thus cannot form a direct association with GNA (Fig 2B). Consistent with this model, matrix-assisted laser desorption ionization/time-of-flight mass spectrometry (MALDI-TOF-MS) analysis further revealed that the m/z ratio of the Cys668-containing peptide Biotin-DKYMCSFLFN was 1,493.5 in the absence of GNA and 2,124.9 in the presence of GNA. Thus, the calculated mass shift of 631.4 was consistent with the covalent addition of one molecule of GNA to the Cys668 residue of EZH2 (Fig 2C).

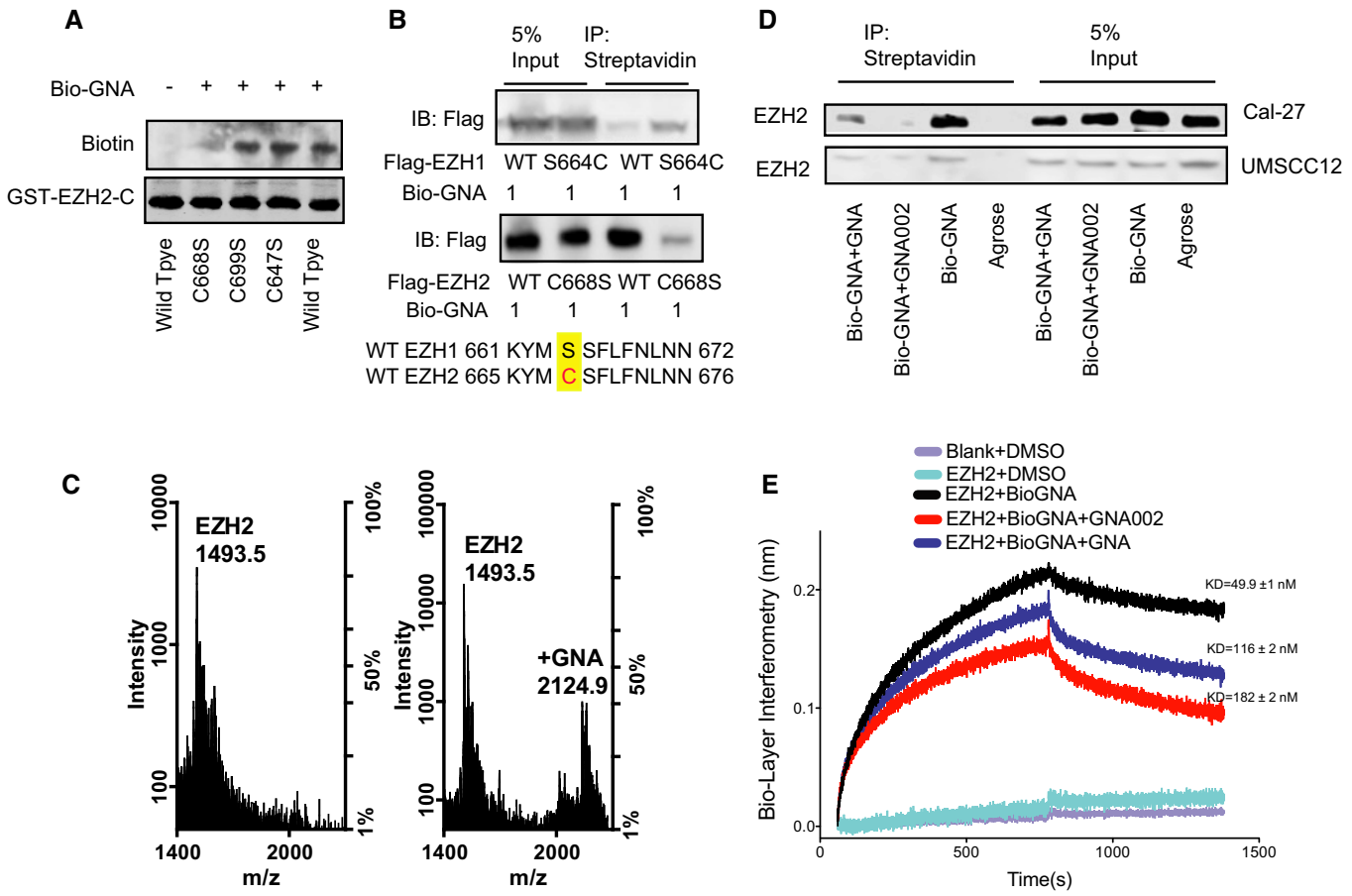

Figure 2. EZH2 covalently binds to GNA and its derivatives.

A Recombinant wild-type (WT) C-terminal EZH2 and its indicated mutants (C688S, C699S, and C647S) were incubated with 5 μM Bio-GNA *in vitro* for 1 h followed by immunoblotting with antibodies against biotin and EZH2.

B Full-length WT and the C668S mutant form of EZH2 (bottom panel) as well as full-length and the S664C mutant form of EZH1 (upper panel) were incubated with 1 μM Bio-GNA *in vitro* for 1 h followed by immunoblotting with antibodies against biotin and EZH2.

C The MALDI-TOF-MS analysis illustrates the direct interaction between GNA and EZH2.

D Immunoblotting assays revealed that Bio-GNA binds to EZH2 in whole-cell lysates derived from Cal-27 and UMSCC12 head and neck cancer cells, whereas free GNA and GNA002 competed with Bio-GNA to bind EZH2.

E The octet assay indicated that GNA and GNA002 could compete with Bio-GNA to bind the bacterially purified recombinant His-EZH2-SET domain. All experiments were performed in triplicate. The data are presented as the mean ± SD (n = 3).

Source data are available online for this figure.

The stability of PRC2 complex components as well as H3K27 trimethylation is decreased by GNA derivatives

To further increase the efficacy of GNA as a more effective EZH2 inhibitor, we synthesized several GNA derivatives (Appendix Table S2) and identified a small molecule, GNA002, as a potentially stronger EZH2 inhibitor than GNA (Fig 2D and E and Appendix Fig S1D). Further evidence from the experimental and computational modelings indicated that GNA002 binds to EZH2 more strongly than GNA (Appendix Fig S2E and F). Notably, GNA002 directly binds to the EZH2 SET domain, as revealed by the liquid chromatography–mass spectrometry (LC-MS) assay (Appendix Fig S2G). As GNA002 is a relatively more potent EZH2 interacting agent than GNA (Fig 2E), we primarily used GNA002 in the following mechanistic and functional studies.

Importantly, we observed that both GNA002 and the previously reported EZH2 inhibitor, GSK126 (McCabe *et al*, 2012), efficiently reduced EZH2-mediated H3K27 trimethylation (Fig 3A). More interestingly, unlike the enzymatic EZH2 inhibitor GSK126, GNA002 led to a dose-dependent reduction in endogenous EZH2 protein abundance (Fig 3A). However, EZH2 mRNA levels were not significantly reduced after GNA002 treatment in both HN-4 and Cal-27 cells, indicating a possible post-transcriptional regulation of EZH2 by GNA002 (Fig 3B). Consistent with previous studies reporting that covalent binding of the small molecular compound affects protein stability (Zhang *et al*, 2010; Titov *et al*, 2011; Zhen *et al*, 2012), we found that the GNA002-induced EZH2 decrease was inhibited by the 26S proteasome inhibitor, MG132 (Fig 3C). This effect was concurrent with an increase in ubiquitination of WT-EZH2, but not by the non-GNA002-interacting, C668S mutant form of EZH2 (Fig 3D). Furthermore, we found that

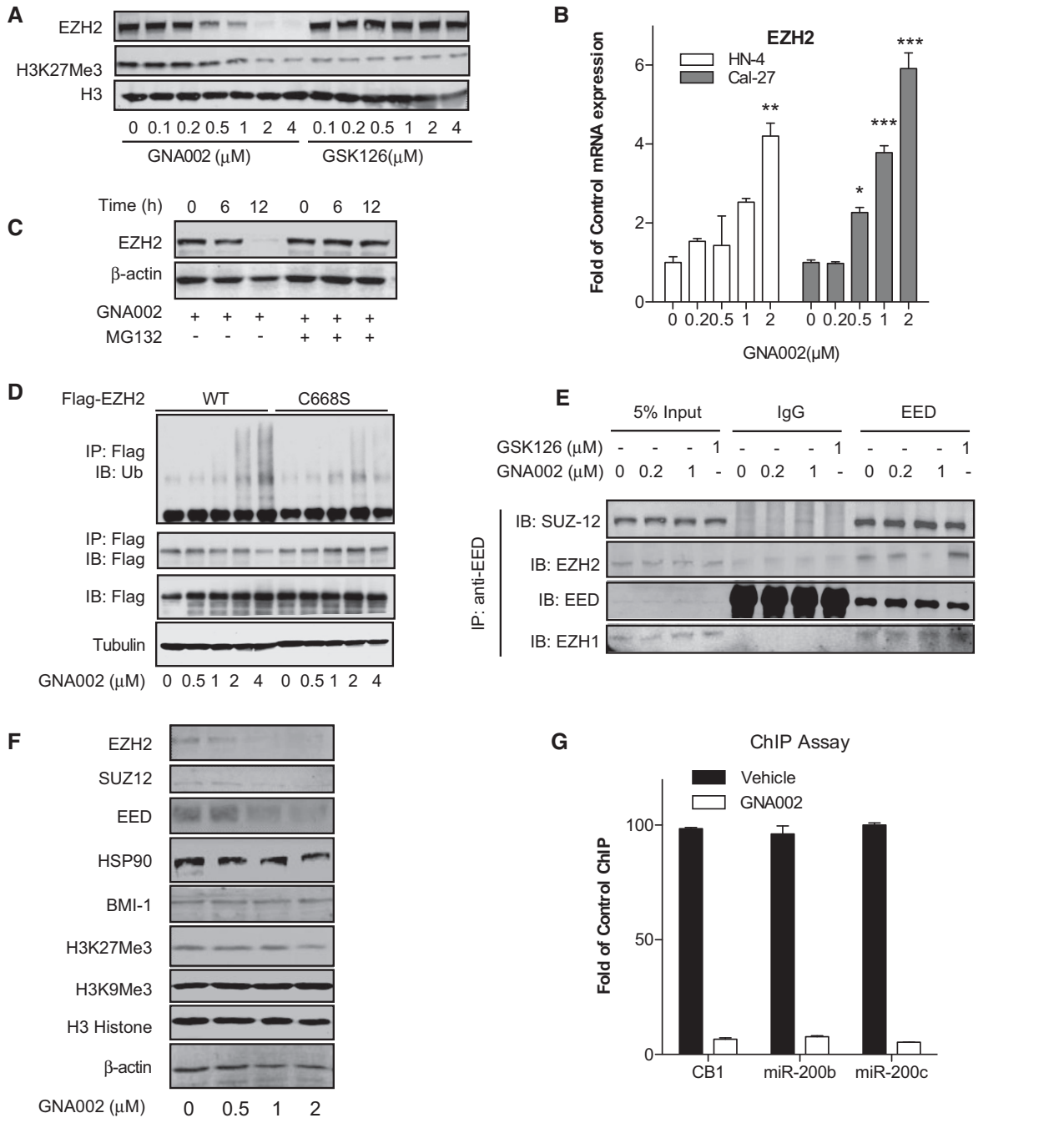

Figure 3. The protein stability of PRC2 complex components and H3K27Me3 are decreased by GNA derivatives.

A Immunoblotting analysis demonstrated that long-term (48 h) incubation of both GNA002 and GSK126 significantly reduced H3K27Me3 levels in Cal-27 head and neck cancer cells. However, GNA002, but not GSK126, led to a significant reduction in EZH2 abundance.

B Treatment with GNA002 for 24 h did not reduce EZH2 mRNA levels in either Cal-27 or HN-4 head and neck cancer cells. The data are presented as the mean fold change of expression ± SEM (n = 3), *P < 0.05, **P < 0.01, ***P < 0.001. Statistical analysis was performed using one way ANOVA method.

C Treatment with the 26S proteasome inhibitor MG132 (5 μM) reversed GNA002 (2 μM)-induced reduction of EZH2 protein levels in Cal-27 cells.

D GNA002 increased the ubiquitination of ectopically expressed, Flag-tagged wild-type EZH2, but not the non-GNA-interacting C668S mutant form of EZH2, as detected by the anti-ubiquitin antibody of the Flag immunoprecipitates recovered from HEK293 cells that were transfected with the indicated plasmids.

E GNA002 treatment for 24 h decreased the association between EZH2 and EED within the PRC2 complex in Cal-27 cells.

F Immunoblotting assays demonstrated that GNA002 treatment (24 h) reduced the abundance of PRC complex components and H3K27Me3 in Cal-27 cells in a dose-dependent manner.

G Cal-27 cells were treated with 2 μM GNA002 for 24 h and subject to ChIP assays to determine the H3K27Me3 status within the promoter regions of characterized EZH2 gene targets, such as CB1, miR-200C, and miR-200C. The experiments were performed in triplicate. The data are presented as the mean ± SD (n = 3).

Source data are available online for this figure.

GNA002 treatment decreased H3K27Me3 levels in UMSCC-12 head and neck cancer cell expressing wild-type EZH2, but not in C668S mutant-expressing UMSCC-12 cells (Appendix Fig S3A and B). Intriguingly, other histone lysine methylation, ubiquitination, and acetylation patterns were not significantly altered by GNA002 treatment (Appendix Fig S3A and B). These data thus demonstrated that GNA002 exerts its biological effect by specifically interacting with and inhibiting EZH2 enzymatic activities.

We next examined the biological consequences of GNA002 on the PRC2 complex and found that GNA002 incubation led to the dissociation of the functional PRC2 complex (Fig 3E) that was coupled to a reduction in the abundance of all of the PRC2 components that we examined after prolonged GNA002 treatment (Fig 3F). Interestingly, the C668S mutant form of EZH2, which is deficient in interacting with GNA derivatives, exhibited resistance to GNA002-induced dissociation of the PRC2 complex (Appendix Fig S3C). Consistent with EZH2 being the catalytic subunit of PRC2, histone H3K27Me3 but not H3K9Me3 levels were strongly reduced in GNA002-treated cells (Fig 3F and Appendix Fig S3D). Notably, GNA002 treatment did not result in an obvious reduction in the abundance of BMI-1, a critical component of the multi-subunit polycomb repressor complex 1 (Fig 3F) that suppresses gene transcription of a faculty of target genes largely by promoting H2A ubiquitination (Cao *et al*, 2005). These results further illustrate the specificity of the GNA derivatives in suppressing EZH2 and PRC2 enzymatic activities in cells, at least in this experimental condition.

Moreover, the levels of EZH2 and SUZ12 but not of other methyltransferases, including ESET or SET8, decreased upon the GNA002 treatment (Appendix Fig S3E), indicating that GNA derivatives specifically decreased the abundance of PRC2 complex components but not other methyltransferases. Similarly, using chromatin immunoprecipitation analysis, we found that GNA002-treated epithelial cancer cells (Cal-27) lost H3K27 trimethylation within the core promoter region of many previously reported EZH2 downstream target genes (Cao *et al*, 2011; Fig 3G). As a result, the mRNA levels of a cohort of characterized EZH2 target genes were significantly reactivated in epithelial cancer cells, such as HN-12 (Appendix Fig S3F), Cal-27 (Appendix Fig S3G), and HN-4 cells (Appendix Fig S3H) after 24 h of incubation with 2 μM GNA002.

EZH2 protein levels are reduced largely through the CHIP E3 ubiquitin ligase

To further pinpoint the molecular mechanism underlying GNA002-induced EZH2 ubiquitination, we next screened for upstream E3 ligase(s) that may potentially mediate EZH2 ubiquitination. To this end, EZH2 protein levels in Cal-27 cancer cells were assessed after the depletion of a series of ubiquitin E3 ligases by siRNA. The knockdown efficiency of the human homolog of Ariadne (HHARI), c-Cbl, Parkin, E6-associated protein (E6AP), and CHIP was examined by real-time polymerase chain reaction (PCR) assays (Appendix Fig S3I). Notably, the depletion of endogenous *CHIP* led to an increase in endogenous EZH2, whereas EZH2 levels upon depletion of other E3 ligases appeared to be relatively unchanged in this experimental setting (Appendix Fig S3J). To further monitor CHIP expression in clinical epithelial cancer samples, immunohistochemical (IHC) assays were performed in cancer tissues versus normal tissues. As presented in Appendix Fig S3K, CHIP expression was relatively increased in cancer tissues compared with normal tissues. Consistently, previously published results have also illustrated relatively increased expression of CHIP in human cancers, such as leukemia (Bonvini *et al*, 2004) and glioma (Xu *et al*, 2011). Hence, the broad expression status of CHIP in various human tumor types supports the potential general utility of GNA derivatives in clinical anti-cancer treatments.

In further support of CHIP as a physiological E3 ligase for EZH2, we observed that CHIP appears to be present in both nucleus and cytoplasm compartments, whereas EZH2 is mostly localized in the nucleus (Fig 4A). Additionally, we found a physical interaction between endogenous CHIP and endogenous EZH2 by co-immunoprecipitation (IP) assays (Fig 4B). Moreover, depletion of endogenous *CHIP* by multiple shRNAs significantly retarded GNA002-induced degradation of endogenous EZH2 in the epithelial cancer cell line UMSCC-12 (Fig 4C). Interestingly, ectopic expression of CHIP required the presence of GNA002 to significantly promote the ubiquitination of EZH2 (Fig 4D). On the other hand, CHIP failed to promote the ubiquitination of the non-GNA-interacting C668S mutant form of EZH2, even in the presence of GNA002 (Fig 4D), further emphasizing the critical role of CHIP in mediating GNA-induced EZH2 ubiquitination, a process that may require GNA covalent bound to EZH2, presenting as a protein misfolding signal. In support of this finding, *in vitro* GST-pull-down assays demonstrated that the WT-EZH2 SET domain, but not the C668S mutant EZH2 SET domain interacts with CHIP only in the presence of GNA002 (Appendix Fig S4A).

Notably, CHIP is a key player of the protein quality control system and mediates the polyubiquitination of misfolded or aggregated proteins for targeted degradation (Whitesell & Lindquist, 2005; Ferreira *et al*, 2013). In further support of this hypothesis, we found that ectopic expression of CHIP efficiently reduced the protein abundance of endogenous EZH2 (Appendix Fig S4B). In addition, consistent with a previous report (Yu *et al*, 2013), we found that depletion of endogenous *Smurf2,* but not *Smurf1,* phenocopies *CHIP* depletion by elevating the basal levels of endogenous EZH2 (Fig 4E). However, unlike *CHIP* depletion, the depletion of endogenous *Smurf2* could not retard GNA002-induced degradation of EZH2 (Fig 4F), further confirming CHIP, but not Smurf2, as the physiological E3 ligase that is largely responsible for triggering EZH2 degradation under the experimental conditions of GNA002 treatment.

Next, we continued to explore the biological effects of inhibiting the EZH2 oncoprotein with this novel class of EZH2 inhibitors. Notably, we found that both GNA and GNA002 clearly inhibited the proliferation of numerous cancer cell lines (Appendix Fig S4C and Appendix Table S3), especially in cancer cells with relatively increased expression levels of EZH2 mRNA and protein (Appendix Fig S4D–G). The anti-cancer effects were mediated, in part, through the induction of cellular apoptosis (Appendix Fig S4H). Consistently, GNA002 demonstrated an elevated capacity to induce cell death in human cancer cells compared with GNA, whereas the inactive GNA derivative, GNA008 (Appendix Fig S1E), was incapable of inducing apoptosis or inhibiting cellular growth (Appendix Fig S4H and Appendix Table S4). These results suggest that the GNA novel class of EZH2 inhibitors most likely exerts their anti-cancer effects by inducing cellular apoptosis through direct interactions with critical targets, such as EZH2, as a Michael acceptor (Appendix Fig S2D; Groll *et al*, 2008; Liu *et al*, 2012).

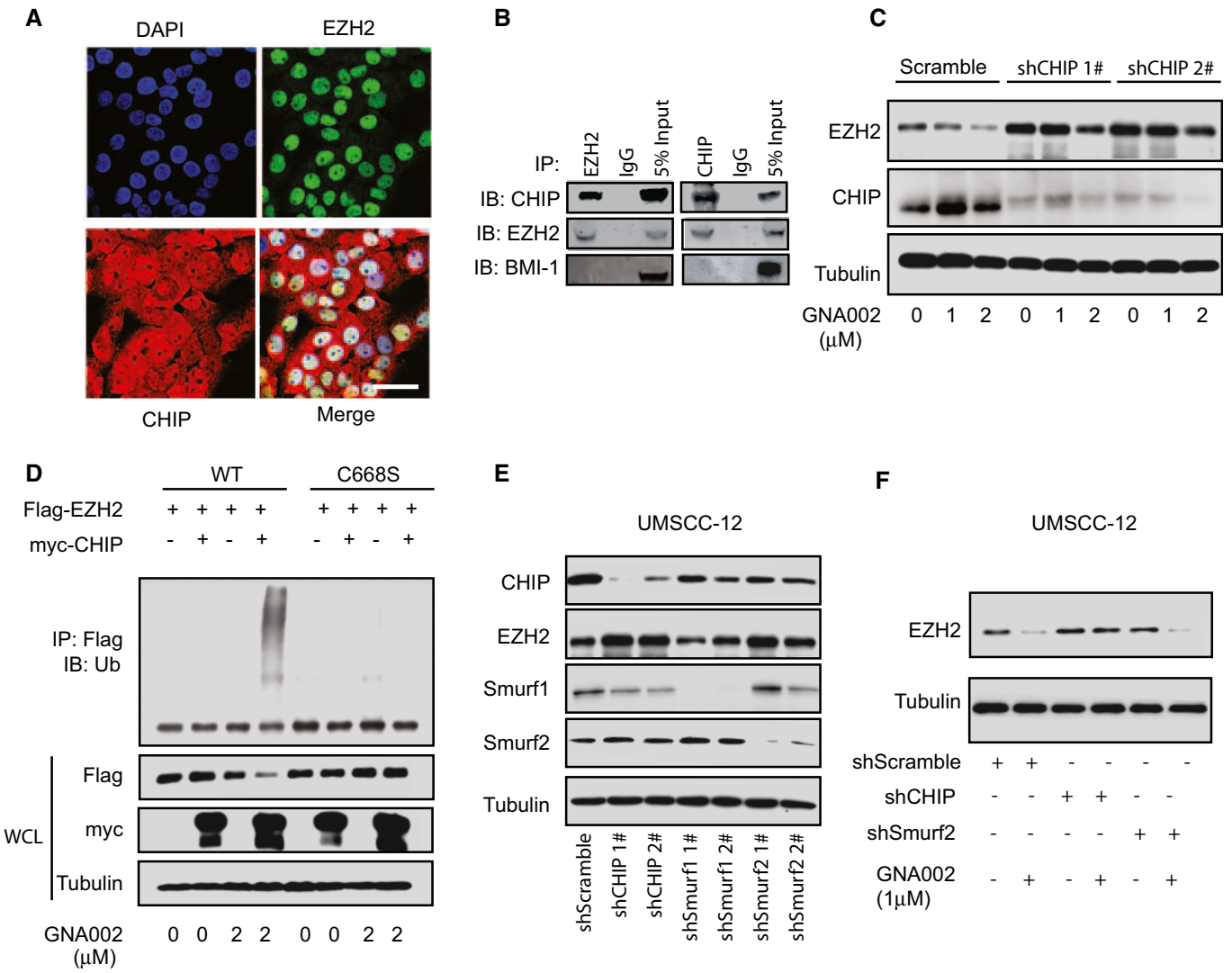

Figure 4. EZH2 protein levels are decreased largely through the E3 ubiquitin ligase CHIP.

A Immunofluorescence analysis indicated that EZH2 and CHIP proteins co-localized in the nuclei of HN-6 head and neck cancer cells. Scale bar, 75 μm.

B Detection of the endogenous interaction between EZH2 and CHIP by co-immunoprecipitation in Cal-27 head and neck cancer cells.

C Immunoblotting analysis demonstrated that the depletion of endogenous *CHIP* using two independent lentiviral shRNA constructs led to elevated basal EZH2 levels and resistance to GNA002-induced EZH2 degradation in UMSCC-12 head and neck cancer cells.

D Ectopic expression of CHIP promoted the ubiquitination of WT-EZH2, but not the non-GNA-interacting C668S mutant EZH2, only when challenged with GNA002 in HEK293 cells for 24 h.

E Immunoblotting analysis to monitor changes in endogenous EZH2 abundance following the lentiviral shRNA-mediated depletion of endogenous *CHIP*, *Smurf1*, or *Smurf2* in UMSCC-12 cells.

F Depletion of endogenous *CHIP*, but not endogenous *Smurf2*, conferred resistance to EZH2 degradation induced by a 48-h GNA002 treatment in UMSCC-12 cells.

Source data are available online for this figure.

In keeping with this notion, GNA002 is more potent than GNA at decreasing the mitochondrial membrane potential (Appendix Fig S4I) to trigger cancer cell death through induction of apoptotic pathways (Appendix Fig S4J). Importantly, consistent with a previous report, we found that the GNA-mediated inactivation of EZH2 led to the elevated expression of the pro-apoptotic protein, Bim (Appendix Fig S4K), which is a well-characterized EZH2 downstream transcriptional target (Wu *et al*, 2010). Furthermore, the depletion of endogenous *Bim* in UMSCC-12 partially inhibited GNA002-induced apoptosis (Appendix Fig S4K), illustrating that Bim is a critical downstream effector for GNA derivative-induced apoptosis. Notably, although CDK1 was previously reported to reduce EZH2 stability (Wei *et al*, 2011; Wu & Zhang, 2011), GNA002 appears to not be involved in this signaling pathway given that unlike EZH2, neither CDK1, Cyclin A nor Cyclin B levels were significantly upregulated by GNA002 treatment (Appendix Fig S4K).

As a previous study reported that GNA treatment also inhibited the AKT signaling pathway (Yu *et al*, 2012), we further examined phosphorylation status of the AKT protein. As shown in Appendix Fig S4L, both shEZH2 lentivirus and GNA002 treatment reduced AKT

phosphorylation. Moreover, GNA002 incubation inhibited AKT phosphorylation only in WT-EZH2-expressing UMSCC-12 cells, but not in C668S mutant-expressing cells (Appendix Fig S4M). On the other hand, the EZH2 enzymatic inhibitor GSK126 did not significantly impact AKT phosphorylation (Appendix Fig S4L and M). These data indicate that EZH2 inactivation inhibits AKT oncogenic signaling, in part contributing to the anti-cancer effects of GNA derivatives.

Moreover, in agreement with CHIP being the physiological E3 ligase governing GNA-induced EZH2 degradation, we observed that CHIP increased the ubiquitination levels of only wild-type EZH2-SET, but not those of the non-GNA-interacting C668S mutant EZH2-SET, in an *in vitro* ubiquitination assay (Appendix Fig S4N). Furthermore, as shown in the cellular IP assays, GNA002 treatment increased the binding of CHIP to wild-type EZH2, but not C668S mutant form of EZH2 (Appendix Fig S3C). We further found that depletion of endogenous *CHIP* increased the GNA002 half-maximal inhibitory concentration (IC_{50}) value. In contrast, ectopic expression of CHIP, conversely, decreased the GNA002 IC_{50} value (Appendix Fig S4O) in Cal-27 cells. Moreover, in GNA002-treated Cal-27 cells, depletion of endogenous *CHIP* (Appendix Fig S4P) inhibited GNA002-induced EZH2-targeted gene expression (Appendix Fig S4Q), thereby restoring cell proliferation (Appendix Fig S4R). On the other hand, ectopic expression of CHIP elevated the suppression of cancer cell proliferation by GNA002, whereas this effect was largely abolished in cells expressing the C668S mutant form of EZH2, which is deficient in associating with GNA derivatives (Appendix Fig S4S). These results together validate the critical physiological role of CHIP in GNA002-mediated anti-cancer effects.

The EZH2 inhibitor significantly suppresses cancer growth in a xenograft mouse model

We next examined the anti-cancer growth effect of GNA002 *in vivo*. To this end, the *in vivo* pharmacokinetic profiling of plasma samples collected for up to 24 h suggested that the oral administration of GNA002 displayed noticeable anti-cancer effects (Appendix Fig S5A–C) at concentrations exceeding IC_{50} values against EZH2 obtained with *in vitro* cell culture models (Appendix Fig S4C and Appendix Table S3). Using a xenograft mouse model, we found that the oral administration of 100 mg/kg GNA002 significantly decreased the size (Fig 5A) and weight (Fig 5B) of tumors formed by Cal-27 cells compared with the control group. On the other hand, a clinical, front-line anti-cancer agent, cisplatin (Galluzzi *et al*, 2012), also exhibited similar anti-cancer effects (Fig 5A), but unfavorably reduced the body weight of the treated nude mice (Fig 5C). Critically, side effects have become a major hurdle in the clinical application of chemotherapeutic agents, such as cisplatin, in human patients with epithelial cancers (Arimidex *et al*, 2006). Notably, we found that GNA002 treatment had no significant influence on mouse body weight (Fig 5C), suggesting the potential for minimal side effects for GNA002 given its specificity for EZH2. In support of this notion, hematoxylin and eosin (H&E) analysis showed that the treatment of nude mice with GNA002 did not induce major morphological changes in the examined organ tissues, including the small intestinal crypts and spleen (Appendix Fig S5D). In contrast, cisplatin induced obvious crypt loss and villous atrophy, suggesting that GNA002 is potentially a more specific and less toxic anti-cancer agent than cisplatin.

Importantly, GNA002 treatment not only decreased the volumes of Cal-27-derived tumors (Fig 5B) but also reduced H3K27Me3 levels in tumor tissues (Fig 5D). Mechanistically, IHC analysis further demonstrated that the oral administration of GNA002, but not cisplatin, strongly reduced EZH2 levels in Cal-27 xenograft tumor tissues. The observed GNA-induced cessation of tumor cell proliferation was further supported by reduced Ki-67-positive staining and increased TUNEL-positive staining in tumor tissues (Appendix Fig S5F). Furthermore, GNA002 also significantly suppressed the *in vivo* tumor growth derived from the xenografted A549 lung cancer cells (Appendix Fig S5E).

Given that the lymphoma cells were more dependent on the EZH2 oncoprotein and gain-of-function mutant-EZH2-expressing lymphoma cells are a more suitable target for EZH2 inhibitors, we also examined EZH2 expression in lymphoma cell lines harboring either wild-type or mutant EZH2 (Appendix Fig S5G). Interestingly, we found that GNA002 significantly reduced the abundance of PRC2 components in both wild-type EZH2-expressing Daudi cells (Fig 5E) and mutant EZH2-expressing Pfeiffer cells (Fig 5G), regardless of EZH2 mutation status. Consistently, GNA002 sufficiently suppressed the xenograft tumor growth of Daudi (Fig 5F) and Pfeiffer (Fig 5H) cells. Moreover, we continued to examine the cellular response of KE-37 cells, a cell line that have been previously demonstrated to grow irregardless of EZH2 activity status, as well as the Pfeiffer cells that are addicted to EZH2 enzymatic activity. Notably, we found that although in both cell lines, GNA002 can reduce EZH2 protein abundance to comparable levels (Appendix Fig S5H), the IC_{50} of KE-37 to GNA and GNA002 is much higher than Pfeiffer cells (Appendix Table S3), indicating that GNA and GNA002 might block cell growth in part by specifically suppressing EZH2 enzymatic activity(Bracken *et al*, 2003). These results together confirm that the newly identified GNA002 is orally bioavailable and accumulates at levels that are sufficient to inhibit the aberrant oncogenic functions of EZH2, thus inhibiting tumor growth *in vivo,* at least in the xenograft experimental model.

Next, given that drug resistance is an obstacle for successful clinical anti-cancer practice (Tiedt *et al*, 2011), we also examined potential mutations in EZH2 that could escape the inhibitory effects of GNA derivatives. To this end, our biochemical analysis and computational modeling (Appendix Fig S6A and B) revealed that EZH2 has one cysteine residue (C668) that is directed outward to provide an appropriate site for the Michael reaction to mediate the covalent bond with GNA and GNA002, whereas other examined methyltransferases do not contain this residue. Strikingly, the non-GNA-interacting (Fig 2A and B) C668S mutation has been detected in human clinical cancer samples (Network, 2012; Appendix Fig S6C), indicating that an acquired C668S mutation in the EZH2 oncoprotein might provide a growth advantage for tumor cells in part by escaping the inhibitory effects of the GNA class of inhibitors. In support of this assumption, we found that the C668S mutant-expressing UMSCC12 cancer cells displayed an elevated resistance to the GNA002-mediated inhibition of anchorage-independent growth (Fig 6A and B). The *in vivo* xenograft tumor model experiments further indicated that cancer cells expressing the non-GNA-interacting C668S mutant displayed significant resistance to GNA002 treatment compared with WT-EZH2-expressing cells (Fig 6E). These results together coherently indicate that GNA

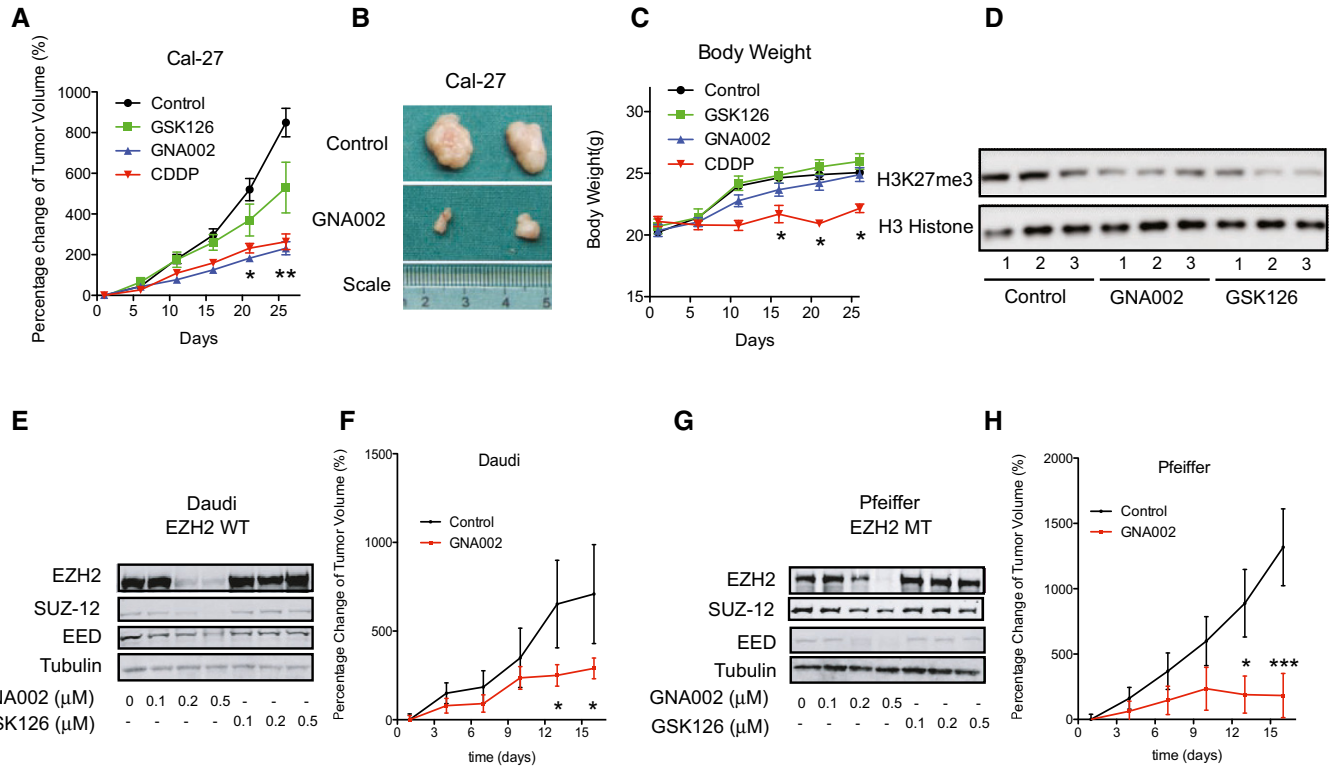

Figure 5. EZH2 degradation induced by GNA derivatives suppresses *in vivo* tumor growth.

A Nude mice bearing Cal-27 xenograft tumors were orally administered GNA002 (p.o., 100 mg/kg, once per day, $n = 10$), GSK126 (i.p., 50 mg/kg, once per day, $n = 10$), cisplatin (i.p., 5 mg/kg, once per week, $n = 10$), or vehicle control (p.o., once per day, $n = 10$). Tumor sizes were measured daily, converted to tumor volume and plotted against days of treatment. The data are presented as the mean percentage change of tumor volume ± standard error of the mean (SEM). $^{*}P < 0.05$, $^{**}P < 0.01$.

B Representative images of the xenografted tumors after vehicle or GNA002 treatments.

C Body weights of the treated mice from (A) were recorded daily after the indicated treatments. The data are presented as the mean ± standard error of the mean (SEM). $^{*}P < 0.05$.

D Oral GNA002 treatment (100 mg/kg) for 4 weeks led to a decrease in H3K27Me3 levels in the collected Cal-27 xenografted tumors.

E Immunoblotting assays indicated that GNA002 incubation for 48 h not only reduced H3K27Me3 levels as GSK126 did, but also significantly reduced the EZH2 protein abundance in the wild-type EZH2-expressing lymphoma Daudi cells.

F Nude mice bearing Daudi xenograft tumors were orally administered GNA002 (p.o., 100 mg/kg, once per day, $n = 10$) or vehicle control (p.o., once per day, $n = 10$). Tumor sizes were measured every 3 days. The data are presented as the mean percentage change of tumor volume ± SEM. $^{*}P < 0.05$.

G Immunoblotting assays indicated that GNA002 incubation for 48 h not only reduced H3K27Me3 levels as GSK126 did, but also significantly reduced mutant EZH2 protein expression in Pfeiffer cells that harbor gain-of-function EZH2 mutation.

H Nude mice bearing Pfeiffer xenograft tumors were orally administered GNA002 (p.o., 100 mg/kg, once daily, $n = 10$) or vehicle control (p.o., once daily, $n = 10$). Tumor sizes were measured every 3 days. The data are presented as the mean percentage change of tumor volume ± SEM. $^{*}P < 0.05$, $^{***}P < 0.001$.

Source data are available online for this figure.

derivatives are specific EZH2 inhibitors by covalently binding to the Cys668 residue within the SET domain.

More importantly, the C668S mutant displayed an enzymatic activity similar to that of WT-EZH2 regarding the maintenance of H3K27 trimethylation *in vitro* (Appendix Fig S6D), arguing that the observed effect of the C668S mutation was largely due to its deficiency in associating with GNA002 rather than directly affecting the methyltransferase activity of EZH2. Given the critical role of CHIP in promoting the destruction of the EZH2 oncoprotein when challenged with GNA002, we also reasoned that the reduced expression of CHIP in human cancers might override the anti-cancer effects on GNA derivatives. In support of this contention, we found that the depletion of endogenous *CHIP* moderately desensitized UMSCC12 cells to GNA002 (Fig 6C and D), thereby leading to an acquired resistance to GNA002 *in vivo* as assessed by a xenograft mouse model (Fig 6F). This effect occurs in part through significantly elevated EZH2 levels and a subsequent increase in H3K27Me3 levels (Appendix Fig S6E).

Discussion

Covalent modifications of specific oncoproteins have recently gained increasing attention as a novel anti-cancer strategy and for drug development (Zhou *et al*, 2009; Kim *et al*, 2013a). To sufficiently decrease the expression level and the oncogenic function of the EZH2 protein in cancer cells, GNA and its derivatives represent a unique category of inhibitor(s) that covalently binds to EZH2, but

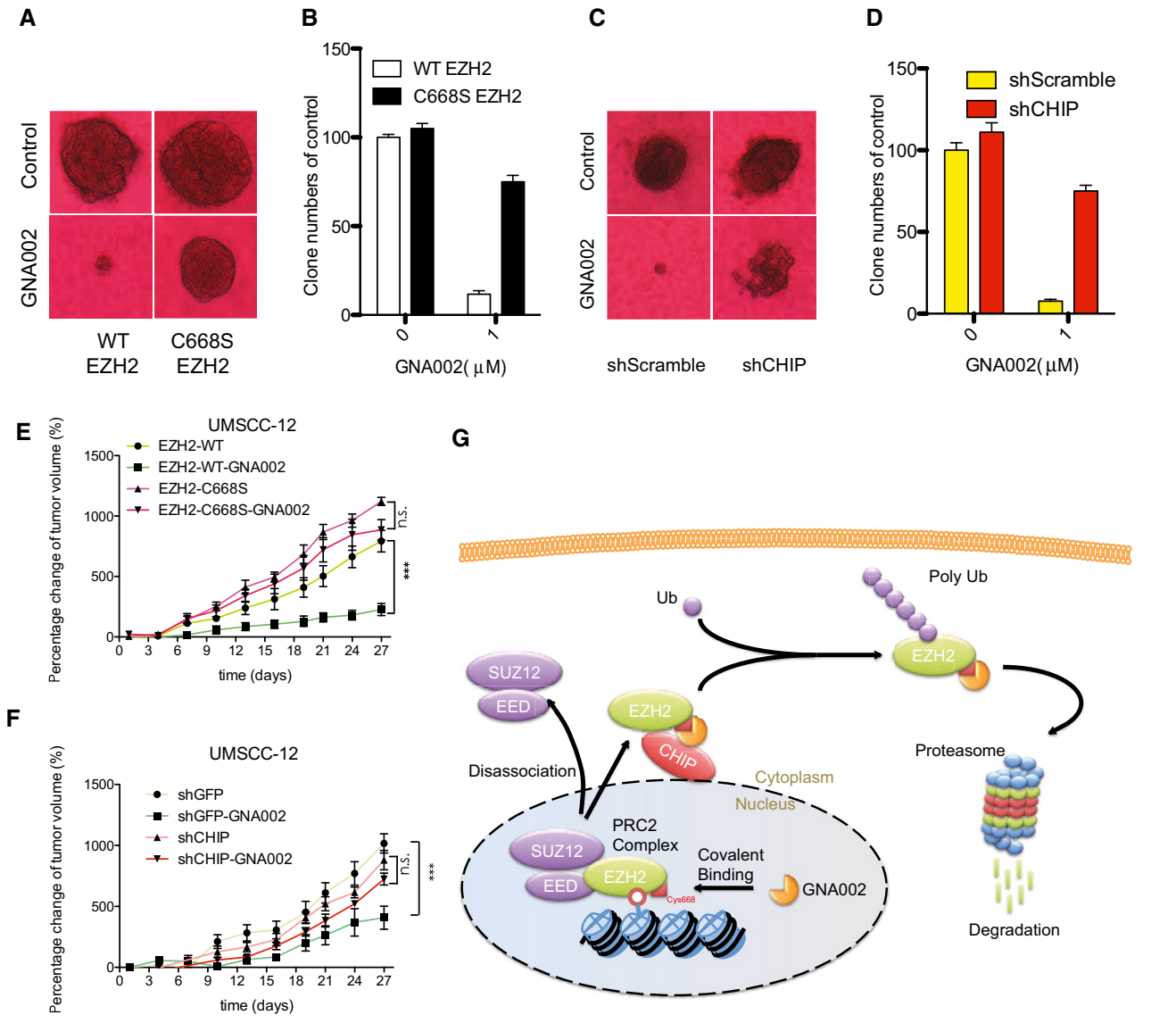

Figure 6. The non-GNA-interacting EZH2-C668S mutant rescues GNA002-induced reduction of tumor growth.

A The anchorage-independent growth of WT-EZH2-expressing but not C668S-expressing UMSCC-12 head and neck cancer cells was retarded by 1 μM GNA002 treatment for up to 6 weeks.

B Quantification of the results that were obtained in (A). The experiments were performed in triplicate. Mean ± SEM.

C Depletion of endogenous *CHIP* in UMSCC-12 cells partially conferred resistance to GNA002-mediated suppression of anchorage-independent growth at the end of 6 weeks.

D Quantification of the results that were obtained in (C). The experiments were performed in triplicate. Mean ± SEM.

E Nude mice bearing WT-EZH2- or C668S-EZH2-expressing UMSCC-12 xenografted tumors were orally administered GNA002 (p.o., 100 mg/kg, once daily, $n = 10$) or vehicle control (p.o., once daily, $n = 10$). The data are presented as the mean percentage change of tumor volume ± SEM. One way ANOVA analysis was used to assess the statistical significance. ***$P < 0.001$.

F Nude mice bearing shGFP- or shCHIP-expressing UMSCC-12 xenograft tumors were orally administered GNA002 (p.o., 100 mg/kg, once daily, $n = 10$) or vehicle control (p.o., once daily, $n = 10$). The data are presented as the mean tumor volume ± SEM, One way ANOVA analysis was used to assess the statistical significance. ***$P < 0.001$.

G A proposed model to illustrate the molecular mechanisms underlying GNA derivatives as a novel class of EZH2 inhibitors. GNA and GNA derivatives specifically interact with EZH2 but not other methyltransferases by forming a covalent bond between the C8 equivalent atom of the GNA derivatives and the S atom of the Cys668 residue in the SET domain of EZH2. Subsequently, GNA binding to EZH2 induces CHIP-dependent polyubiquitination and the subsequent degradation of EZH2, thereby leading to a total termination of the EZH2 oncogenic functions in human cancer cells.

not to the other methyltransferases that we examined. We found that this strategy is an effective method to terminate the oncogenic functions of EZH2 both *in vivo* and *in vitro*. Notably, recent studies have begun to reveal that the oncogenic functions of EZH2 are dependent on its histone methyltransferase activity as well as its role as a co-activator for critical transcription factors that promote tumorigenesis (Sparmann & van Lohuizen, 2006; Shih *et al*, 2012). We discovered that EZH2 degradation was induced by GNA

derivatives in part by directly binding to EZH2. Biochemical analysis allowed us to further identify Cys668 as the single residue located in the SET domain of EZH2 to form a covalent bond with the C8 equivalent atom of GNA and GNA derivatives. Although previously the EZH2 inhibitor DZNep was also reported to induce the degradation of the oncoprotein EZH2 (Tan *et al*, 2007), the underlying mechanism of GNA002 is very different from that of DZNep. Specifically, DZNep functions as an analog of methyl group donor, while GNA002 could covalently bind with specific cysteine residue of EZH2 to trigger its ubiquitination and subsequent degradation by the protein quality control E3 ligase, CHIP.

Strikingly, the C668S mutation of EZH2 has been reported in colon cancer clinical samples (Network, 2012). We also found that the C668S mutant form of EZH2 failed to interact with GNA and GNA derivatives. As indicated in Appendix Fig S3A, the levels of H3K27Me3 of C668S-mutant UMSCC-12 cells are not obviously changed compared to the wild type of UMSCC-12 cells. These data suggest that the C668S mutation might function as a passenger mutation, but patients harboring such a mutation may not benefit from clinical treatment with GNA002. As a biological consequence, cancer cells expressing the C668S-EZH2 mutant were more resistant to GNA derivative-induced growth inhibition both *in vitro* and *in vivo*. Hence, our study has clearly defined a target patient sub-population bearing the C668S mutation in EZH2 who might not be suitable for GNA derivative treatment, although patients carrying the C668S EZH2 mutation only accounted for a very small proportion.

However, our mechanistic studies indicate that the accurate exclusion of these resistant patients against GNA002 treatment could enhance the clinical efficacy, which is consistent with the concept of precision medicine (Stadler *et al*, 2014). Furthermore, we pinpointed the signaling pathway involved in the upstream E3 ubiquitin ligase CHIP that governs GNA-mediated ubiquitination and degradation of the EZH2 oncoprotein. Although previous studies have reported that dissociated PRC2 components can be degraded by the proteasome pathway (Yu *et al*, 2013), the identity of E3 ligase(s) remains largely elusive. We demonstrated that depletion of either *Smurf2* or *CHIP* led to increased endogenous EZH2 levels. However, only the depletion of endogenous CHIP conferred cell resistance to GNA-mediated degradation of EZH2.

Recently, lenalidomide-bound Cullin 4-Cereblon E3 ligase acquired a "glue" ability to promote the ubiquitination of IKZF1 and IKZF3 as novel downstream substrates to block myeloma cell growth (Kronke *et al*, 2014; Lu *et al*, 2014). In our discovery, the novel "glue" effects between CHIP-mediated degradation and the EZH2 oncoprotein were triggered by GNA and its derivatives at the substrate level. This special feature of the target ubiquitination and degradation of EZH2 might be a promising alternative anti-cancer strategy in treating patients with elevated EZH2 enzymatic activity, especially those with aberrant EZH2 overexpression. The covalent binding role and thorough suppression of its full oncogenic function were validated by *in vitro* and *in vivo* experiments both in wild-type EZH2 solid tumors and in the gain-of-function mutant form of EZH2 in lymphomas. Moreover, this novel mechanism distinguishes these potent agents from the currently available EZH2 enzymatic inhibitors.

Additionally, our study demonstrated that covalent binding to the Cys668 residue of the EZH2 SET domain is a promising method of modulating the EZH2 oncoprotein stability following ubiquitination and proteasome-mediated degradation. We also present GNA and its derivatives as novel EZH2-modulating candidates. In this study, we primarily used GNA and the more active GNA002 derivative to illustrate the novel anti-EZH2 strategy. GNA possesses some toxic activity, such as the inhibition of Cdk4/Cyclin D1, AKT, and p38 (Yan *et al*, 2011) and the induction of GSK3β-dependent G1 arrest (Yu *et al*, 2012). However, our current studies demonstrated that under our experimental conditions, GNA and, to a greater extent, its derivative GNA002 specifically inhibit EZH2 but not the other methyltransferases that we examined through the covalent inhibition of a specific cysteine of EZH2. These results indicate that these potent agents against EZH2-C668 act uniquely and independently of other potential anti-cancer mechanisms. Based on our discovery, other chemical compounds can been designed and developed as more specific EZH2 modulators.

In summary, we have uncovered the molecular mechanism underlying the covalent binding of EZH2 to potent agents as well as the signaling pathway(s) for the CHIP-mediated polyubiquitination of the covalently bound EZH2 oncoprotein (Fig 6G). More importantly, we utilized a combination of *in vitro* and *in vivo* assays to validate the novel mechanisms of EZH2 degradation, thereby uncovering a novel method to develop new anti-EZH2 agents as promising anti-cancer therapies.

Materials and Methods

Cell culture

The human head and neck cancer cell lines UMSCC-12 and SCC-25 as well as breast cancer cell lines MDA-MB-231, MDA-MB-468, and MCF-7 and their drug-resistant variant MCF-7/ADM were obtained from the American Type Culture Collection. The human head and neck cell lines HN-4, HN-6, HN-12, HN-13, HN-30, Cal-27, KB, and KB/VCR; the hepatocyte carcinoma cell line SMMC-7721; and the cervical cancer cell line HeLa were obtained from NIH. These cells were maintained in Dulbecco's minimum essential medium (Invitrogen) that was supplemented with 10% fetal bovine serum, 100 units/ml penicillin, and 100 μg/ml streptomycin. MV4-11, RS4-11, Reh, Daudi, Pfeiffer, and KE-37 were obtained from the American Type Culture Collection and cultured with RPMI-1640 medium and 10% fetal bovine serum (Invitrogen). The indicated cell lines were incubated in a humidified atmosphere with 5% CO_2 at 37°C.

Computational modeling

The structural of the EZH2 CXC-SET domain (PDB: 4MI0) was used for covalent binding. The covalent binding mechanism was determined using software Autodock 4.2 (Morris *et al*, 2009). The GNA derivatives were manually docked into the coordinated center of covalent binding site ($x = 30$, $y = 30$, $z = 30$).

Furthermore, protein residue conservation analysis was performed with the ConSurf Web site (Ashkenazy *et al*, 2010), which is publically available at http://consurf.tau.ac.il. The EZH2 mutation was identified in the Cosmic (catalog of somatic mutations in cancer) Web site (Forbes *et al*, 2011), which is publically available at http://cancer.sanger.ac.uk/cancergenome/projects/cosmic/.

MALDI-TOF analysis

The biotinylated EZH2 peptide (Biotin-DKYMCSFLFN) was synthesized by Shanghai Sangon Co. Ltd. Bacterially purified recombinant GST-EZH2 proteins were incubated with GNA or GNA002 for 1 h at 37°C. The molecular weight (MW) of proteins and adducts was recorded with the MALDI-TOF Mass Spectrum (Shanghai Applied Protein Technology Co. Ltd.).

Cell growth and survival assays

Cell viability was assessed using the MTT assay (Sigma). Cells were seeded in 96-well micro-culture plates for 12 h to allow for cell attachment before being incubated for an additional 72 h with various concentrations of the tested compounds. Afterward, the MTT reagent was added to each well, and the cells were incubated for 4 h. Then, the colored formazan products were quantified photometrically at 490 nm using a multi-well plate reader (Bio-Rad Laboratories).

Plasmids

The wild-type Myc-CHIP constructs were kindly provided by Dr. Jing Yi (Yan *et al*, 2010; Shanghai Jiao Tong University, School of Medicine, Shanghai, P.R. China). The His-EZH2 expression vector was purchased from Neobio, China. The N-terminal GST- or His-tagged EZH2 wild-type and deletion mutants were described previously (Kaneko *et al*, 2010). The mammalian expression constructs for Flag-tagged wild type and various mutants of EZH2 were also described previously (Cao *et al*, 2013). The EZH2 mutants wherein residues C668, C699 or C647 were replaced by serine were generated with site-directed mutagenesis (Agilent) according to the manufacturer's instructions. The shSmurf1, shCHIP, and shSmurf2 lentiviral constructs were purchased from Open Biosystems. The shBim and shEZH2 lentiviral constructs were purchased from Addgene. Synthesized siRNAs or mammalian expression vectors were transfected into cells at 40–60% confluence using the Lipofectamine 2000 reagent according to the manufacturer's instructions.

Reverse-transcriptional–polymerase chain reaction and quantitative PCR assays

HN-4 and Cal-27 cells were treated with GNA002 at 0, 0.2, and 0.5 μM for 24 h, and quantitative PCR was performed using the ABI Prism 7300 system (Applied Biosystems, Foster City, CA, USA) and SYBR Green (Roche, Mannheim, Germany). For PCR, up to 1 μl of cDNA was used as a template. The thermal cycling conditions were 95°C for 10 min followed by 40 cycles of 95°C for 15 s and 60°C for 30 s. A primer efficiency of > 90% was confirmed with a standard curve spanning four orders of magnitude. Following the reactions, the raw data were exported using the 7300 System Software 4 v1.3.0 (Applied Biosystems) and analyzed.

The primers were as follows: β-actin, sense 5′-ACC AAC TGG GAC GAC ATG GAG AAA-3′ and antisense 5′-TAG CAC AGC CTG GAT AGC AAC GTA-3′; EZH2, sense 5′-TGC AGT TGC TTC AGT ACC CAT AAT-3′ and antisense 5′-ATC CCC GTG TAC TTT CCC ATC ATA AT-3′; miR-200b, sense 5′-CAT CTT ACT GGG CAG CAT TG-3′ and antisense 5′-GTC ATC ATT ACC AGG CAG TAT TAG-3′; miR-200c, sense 5′-CTC GTC TTA CCC AGC AGT GT-3′ and antisense 5′-GTC ATC ATT ACC AGG CAG TAT TAG-3′; c-Cbl, sense 5′-GGA CCA GTG AGT TGG GAG TTA TTA CT-3′ and antisense 5′-GGC AAG ACT TCA CTG TGA AGT CA-3′; CHIP, sense 5′-TGT GCT ACC TGA AGA TGC AG-3′ and antisense 5′-TGT TCC AGC GCT TCT TCT TC-3′; E6AP, sense 5′-AGG AGC AAG CTC AGC TTA CCT-3′ and antisense 5′-CAG CAG CAG AAC ATG CAG C-3′; HHARI, sense 5′-GCT ACG AGG TGC TCA CG-3′ and antisense 5′-ATC CTG TGC TGA TGA CCT TG-3′; and Parkin, sense 5′-CCA GAT TGC CAC CAT GTT GT-3′ and antisense 5′-CAC TGT CAT CAT CAC ACT-3′.

Antibodies

The antibodies that were used in this study were as follows: mouse monoclonal antibody against EZH2 (612667, BD Science); rabbit polyclonal antibody against SUZ-12 (20366-1-AP, Proteintech, USA); mouse monoclonal antibody against β-actin (ab6276, Abcam, USA); rabbit polyclonal antibody against H3K27Me3 (07-449, Millipore, USA); rabbit polyclonal antibody against H3K9Me3 (05-1242, Millipore, USA); rabbit polyclonal antibody against H3 histone (AH433, Beyotime, China); rabbit polyclonal antibody against EED (16818-1-AP, Proteintech); rabbit polyclonal antibody against BMI-1 (10832-1-AP, Proteintech); rabbit polyclonal antibody against PARP (AP102, Beyotime, China); rabbit polyclonal antibody against caspase-8 (13423-1-AP, Proteintech, USA); rabbit polyclonal antibody against caspase-3 (19677-1-AP, Proteintech, USA); rabbit polyclonal antibody against Bcl-2 (12789-1-AP, Proteintech, USA); rabbit polyclonal antibody against Bax (50599-2-Ig, Proteintech, USA); the rabbit polyclonal antibody against ubiquitin (1646-1, Epitomics, USA); mouse monoclonal antibody against Smurf1 (sc-100616, Santa Cruz, USA); rabbit polyclonal antibody against Smurf2 (sc-25511, Santa Cruz, USA); rabbit monoclonal antibody against Bim (2933, Cell Signal, USA); and mouse monoclonal antibody against Flag (F1804, Sigma, USA); Methyl-Histone H3 Antibody Sampler Kit (9847, Cell Signal, USA); Tri-Methyl-Histone H3 Antibody Sampler Kit (9783, Cell Signal, USA); Rabbit polyclonal antibodies against H4K20 methylation (ab9051, ab9052, ab9053, Abcam, USA); Rabbit polyclonal antibodies against EZH1(A5818, Abclonal, China).

Immunofluorescence and immunohistochemistry assays

To visualize the effects of GNA002 on the intracellular retention of Rhodamine 123 (Rho123), 1×10^4 HN-4 cells were seeded on Lab-Tek 8-well chamber slides the day prior to the assay. The cells were then incubated with 0.25 μM Rho123 either alone or in the presence of 2 μM GNA002 in DMEM for 12 h at 37°C. Afterward, the cells were fixed with 4% paraformaldehyde. Nuclear staining was achieved by incubating cells in DAPI for 5 min. The slides were then washed and imaged using a laser-scanning confocal microscope (TCS SP2, Leica, Germany; He *et al*, 2009).

Monolayers of HN-6 cells were fixed with 4% paraformaldehyde, permeabilized with 0.2% Triton X-100, and blocked with 5% bovine serum albumin (BSA) before incubating with antibodies against EZH2, CHIP, or biotin for 2 h at 37°C. Subsequently, cells were incubated with a fluorescein isothiocyanate (FITC)-conjugated secondary antibody (ZYMED, S. San Francisco, CA, USA) for 2 h at 37°C. The cells were then examined by a laser confocal microscope (TCS SP2, Leica, Germany).

Chromatin immunoprecipitation (ChIP) assays

ChIP assays were performed as previously described (Chopra *et al*, 2011; Davalos-Salas *et al*, 2011). Cal-27 cells were treated with or without GNA002 (2 μM) for 24 h. ChIP assays were performed using EZ ChIP kit (Millipore). Briefly, Cal-27 cells (1×10^7 cells) were fixed with 1% formaldehyde and then neutralized by adding 0.125 M glycine. Cells were collected and lysed in cell lysis buffer containing SDS and a cocktail of protease inhibitors. The lysates were sonicated to obtain soluble chromatin with an average length of 1,000 bp. After a 1:10 dilution in dilution buffer, the chromatin solutions were pre-cleared and incubated with IgG or anti-H3K27Me3 antibodies. Next, the mixtures were incubated overnight at 4°C on a rotating platform. The immunocomplexes were captured by protein A/G-Sepharose beads. After extensive washing, the bound DNA fragments were eluted, and the resulting DNA was subjected to real-time qPCR analysis using the following ChIP primer pairs: miR-200a,b, sense 5′-CGT CTG GCC AGG ACA CTT-3′ and antisense 5′-AAT GCT GCC CAG TAA GAT GG-3′; miR-200c, sense 5′-AGG GCT CAC CAG GAA GTG T-3′ and antisense 5′-CCA TCA TTA CCC GGC AGT AT-3′; CB_1, sense 5′-GCA GAG CTC TCC GTA GTC AG-3′ and antisense 5′-AAC AGG CTG GGG CCA TAC AG-3′; and GAPDH, sense 5′-TAC TAG CGG TTT TAC GGG CG-3′ and antisense 5′-TCG AAC AGG AGG AGC AGA GAG CGA-3′.

RNA interference and transfection

RNA interference oligonucleotides were transfected with Lipofectamine 2000 as previously reported (Yan *et al*, 2010). siRNA oligonucleotides were synthesized by Gene Pharma, China. The siRNA sequences were as follows: negative control, sense 5′-UUC UUC GAA CGU GUC ACG UTT-3′ and antisense 5′-ACG UGA CAC GUU CGG AGA ATT-3′; EZH2, sense 5′-GAA UGG AAA CAG CGA AGG ATT-3′ and antisense 5′-UCC UUC GCU GUU UCC AUU CTT-3′; c-Cbl, sense 5′-GGA GAC ACA UUU CGG AUU A dTdT-3′ and antisense 5′-UAA UCC GAA AUG UGU CUC C dTdT-3′; E6AP, sense 5′-GUA GAG AAA GAG AGG AUU A dTdT-3′ and antisense 5′-UAA UCC UCU CUU UCU CUA C dTdT-3′; HHARI, sense, 5′-CGA ACA CGC CAG AUG AAU A dTdT-3′ and antisense, 5′-UAU UCA UCU GGC GUG UUC G dTdT-3′; CHIP, sense, 5′-AGG CCA AGC ACG ACA AGU A dTdT-3′ and antisense 5′-UAC UUG UCG UGC UUG GCC U dTdT-3′; Parkin, sense 5′-GGA AGG AGC UGA GGA AUG A dTdT-3′ and antisense 5′-UCA UUC CUC AGC UCC UUC C dTdT-3′; and CHIP (3′UTR), sense 5′-GAC GUG CUG GUG UGU GAA A dTdT-3′ and antisense 5′-UUU CAC ACA CCA GCA CGU C dTdT-3′.

Cell cycle analysis

The cell cycle distribution of cancer cells was determined as previously reported (Yan *et al*, 2010). HN-4 and Cal-27 cells were seeded in 6-well plates at a density of 2.5×10^5 cells/well overnight. On the following day, the cells were treated with vehicle (DMSO) or 1 μM GNA002 for 24 h. The cells were then trypsinized, and fixed cells were incubated with 0.5 ml of PI/RNase staining buffer for 15 min at room temperature (RT). The DNA content and cell cycle distribution were assessed by the FACScan laser flow cytometry. The data were analyzed using MODFIT and CELLQUEST software.

Flow cytometric analysis for detecting cellular apoptosis

Cancer cells were treated with 2 μM GNA or GNA002 for 24 h. The cells were then harvested and re-suspended with 500 μl of binding buffer. The cell suspension (100 μl) was incubated with 5 μl of annexin V and propidium iodide at RT for 20 min. The stained cells were analyzed with fluorescent-activated cell sorting using the BD LSR II flow cytometry machine (Becton Dickinson, San Jose, CA, USA).

Measurements of mitochondrial membrane potentials ($\Delta\psi m$)

As a previous study reported (Ferlini & Scambia, 2007), the cells were harvested and re-suspended with 500 μl of binding buffer for 20 min after the cancer cells were treated with GNA or GNA002 for 24 h. The stained cells were then analyzed with fluorescent-activated cell sorting using the BD LSR II flow cytometry machine (Becton Dickinson, San Jose, CA, USA).

Immunoblotting analysis

The cells were lysed in lysate solution, and the proteins were separated on 8, 10, or 12% SDS–PAGE gels and transferred to nitrocellulose membranes. Next, 5% milk powder-containing buffer was used to reduce the non-specific background. Bands were detected using various antibodies as indicated. The membranes were incubated with the primary antibodies at 4°C overnight and secondary antibodies for 2 h at RT before using the Odyssey® Infrared Imaging System (Bioscience) or exposure to X-ray film in the dark for band detection.

Immunoprecipitation (IP) and denaturing IP analysis

Cells were harvested using IP buffer (1% Triton X-100, 150 mM NaCl, 10 mM Tris, pH 7.4, 1 mM EDTA, 1 mM EGTA, pH 8.0, 0.2 mM sodium orthovanadate, 1 mM phenylmethanesulfonyl fluoride (PMSF), 0.5% protease inhibitor cocktail, and 0.5% IGEPAL CA-630). Cell lysates were centrifuged at 16,000 *g* for 30 min at 4°C, and the supernatants were incubated with specific antibodies as indicated overnight at 4°C followed by incubation with protein A/protein G-coated agarose beads (Merck) for an additional 4 h at 4°C. After the samples were washed thrice with ice-cold IP buffer and the supernatants were removed by centrifugation at 2,000 *g* for 1 min, the proteins were precipitated individually or co-precipitated. The proteins were then separated from the beads using immunoblotting loading buffer for 5 min at 95°C. The supernatants were collected for subsequent immunoblotting analysis after SDS gel separation.

Denaturing co-IP was performed to detect the ubiquitin conjugations of EZH2 *in vivo*. Cells were lysed in 100 μl of denaturing buffer (100 mM Tris–HCl, 2% SDS, 10% glycerol) before being harvested. After boiling for 10 min, cell lysates were centrifuged for 5 min at RT. Supernatants were mixed with EBC buffer [(50 mM Tris pH 7.5, 120 mM NaCl, 0.5% NP-40) buffer supplemented with protease inhibitors (Complete Mini, Roche) and phosphatase inhibitors (phosphatase inhibitor cocktail set I and II, Calbiochem)] and incubated with Flag-M2 beads (A2220, Sigma). The proteins were separated from the beads using

immunoblotting loading buffer specifically containing 50 mM dithiothreitol (DTT) for 5 min at 95°C. The supernatants were collected for subsequent immunoblotting analysis with the indicated antibodies.

Pull-down of gambogenic acid-bound proteins for HPLC/MS/MS analysis

Biotin- or biotin-gambogenic acid-conjugated agarose beads were prepared as previously described (Shen *et al*, 2009). HN-12 cells were harvested and lysed in RIPA buffer supplemented with various protease and phosphatase inhibitors (Calbiochem, Darmstadt, Germany) with brief sonication. After centrifugation at 12,000 *g* for 30 min, the supernatants (2 mg/ml) were collected and equally divided into four parts, two of which were pre-incubated with unlabeled GNA (10-fold or 20-fold of biotin-labeled GNA) and then incubated with 100 μl of biotin, biotin-GNA-beads, or biotin-GNA-beads in the presence of unlabeled GNA in RIPA buffer overnight at 4°C. After incubation, the beads were washed five times with RIPA buffer, the bead-bound proteins were eluted, the proteins were separated by SDS–PAGE, and the bands were visualized by silver staining. The protein fragments were recorded with the HPLC/MS/MS analysis (Shanghai Applied Protein Technology Co. Ltd.).

CHIP *in vitro* ubiquitination activity assays

CHIP activity was performed using a commercial kit following the manufacturer's instructions (Boston Biotechnology, USA). Glow-Fold™ control protein is progressively ubiquitinated using the reagents and protocol conditions that were supplied in this kit. Ubiquitinated Glow-Fold™ products are visible via immunoblotting; anti-ubiquitin antibodies may detect the targets in addition to polyubiquitinated substrate proteins.

Fortebio octet assay

The interaction between EZH2-SET and compounds was tested by the ForteBio Octet System according to the manufacturer's instructions (ForteBio, Inc., USA). The 10 μM Bio-GNA was immobilized onto Super Streptavidin Biosensors for 30 min at 25°C. The 10 μM recombinant protein of EZH2-SET was prepared in SD buffer (1× phosphate-buffered saline (PBS), 0.02% Tween-20, 0.1% BSA) in the presence of DMSO, GNA (10 μM) or GNA002 (10 μM). The association and dissociation of the EZH2-SET were monitored in parallel to minimize time. The competing binding of compounds to EZH2-SET in the coated and uncoated reference sensors was measured over 1,400 s. This analysis accounts for non-specific binding, background, and signal drift and minimizes well-based and sensor variability.

High-content screening assay

At 24 h after incubation with a library composing of different compounds, the cells were fixed with formalin and washed thrice with PBS. The library consists of natural compounds from previously reported Chinese traditional medicine. We selected these compounds that are highly bio-active and most of them are used in the ancient formula to treat cancer in China. After the cells were incubated with a primary anti-EZH2 antibody (1:300) and a secondary fluorescent antibody (1:200), DNA/nuclei were stained with DAPI (5 μg/ml) that was diluted in blocking solution. The plates were incubated for 1 h at room temperature in the dark.

According to previous studies reported (Adams *et al*, 2014; Martin *et al*, 2014), the plates were imaged using a PerkinElmer Operetta high-content wide-field fluorescence imaging system coupled to Harmony software. The plates were barcoded with specific information, and the barcodes were read before loading onto the Operetta. The wells were imaged using a 40× objective lens in a single focal plane across each plate. The bottom of each well was detected automatically by the Operetta focusing laser, and the focal plane was calculated relative to this value. DAPI emission (455 nm) was imaged for 50 ms. A total of 8 fields of view were imaged per well, with an identical pattern of fields being used in every well. This pattern was designed to avoid imaging cells in the area that was targeted by the dispensers.

Modified Columbus (PerkinElmer) image analysis algorithms were used throughout. Nuclei were detected using a modified "find nuclei" algorithm as blue (DAPI) fluorescent regions > 100 μm^2, with a split factor of 7.0, an individual threshold of 0.40, and a contrast > 0.10 (method B). The phenotypic nuclear spots that are characteristic of EZH2 were detected using a modified "find spots" algorithm as well as using fluorescent spots with a relative spot intensity > 0.030 and a splitting coefficient of 1.0 (method A). Key output parameters were the number of whole nuclei and the percentage of nuclei with EZH2.

Statistical analyses were performed on a plate-by-plate basis using the *z*-score calculation. The strictly standardized mean difference (SSMD) was chosen as the quality control metric to evaluate the variability of and the difference between the control populations. The threshold was set at 0.38 relative to the original EZH2 protein abundance to identify top-hit compounds, which will be further validated by subsequent immunofluorescent and immunoblot assays.

Pharmacokinetic study

The protocol is based on the previous report (Cai *et al*, 2011). Adult male ICR mice were fasted overnight prior to drug administration. GNA002 was administered as a single dose of 12 mg/kg by tail vain injection or oral gavage. At pre-dose and at 0.083, 0.25, 0.5, 1, 2, 4, 8, and 24 h post-dose, blood was collected from three male mice and immediately processed for plasma by centrifugation for 10 min at 3,000 *g*. The resulting plasma was frozen on dry ice, and the samples were stored at −80°C until analysis. Proper measures were taken to minimize pain and discomfort experienced by the mice. The experimental procedures were in accordance with the National Institutes of Health Guide for Care and Use of Laboratory Animals (revised 1996). The experiments were performed in compliance with ethical regulations, and the protocols were approved by the institute's committee. For mouse plasma sample analysis for GNA002, a 0.1-ml aliquot of plasma sample was treated with 0.3 ml of methanol containing 250 nM (internal standard, IS) for direct deproteinization. After vortex mixing for 1 min and centrifuging for 5 min at 10,000 *g*, 0.2 ml of supernatant was transferred to a sample vial, and 5 μl of the sample was injected onto the LC/MS/MS. The LC was performed on an Agilent 1200 HPLC system

(Agilent Technologies, Inc., USA), and separation was performed at 30°C using an Xterra column (2.1 × 50 mm, 3.5 μm; Waters, USA).

The mobile phase consisted of 0.1% formic acid in water–methanol (45:55, v/v), and the flow rate was 0.3 ml/min. The HPLC system was interfaced to an Agilent 6410 triple-quadrupole mass spectrometer (Agilent Technologies, Inc., USA) with an electrospray interface (ESI). The ESI source parameters were as follows: high-purity drying-gas (N2) flow rate, 8 l/min; temperature, 350°C; capillary voltage, 4,000 V; and nebulizer pressure, 30 psi. Multiple reaction monitoring (MRM) was used to quantify GNA002 (*m/z* 732.6, [M+H]+à608.6 fragmentor 150 eV, collision energy −69 eV) and IS (m/z 274.9, [M+H]+à201.8 fragmentor 150 eV, collision energy −40 eV). Data analysis was performed using the MassHunter software package (Agilent Technologies, Inc., USA) containing both qualitative and quantitative software. Plasma standard curves ranged from 2.5 to 1,000 ng/ml. The curves were fitted with a linear regression equation. Concentrations of GNA002 < 2.5 ng/ml were reported as BQL (below the quantification limit of the method). To determine the pharmacokinetic parameters, plasma concentrations versus time data for GNA002 were analyzed by standard noncompartmental methods using the WinNonlin Pro 6.1 software (Pharsight Corporation, Mountain View, CA, USA). Concentrations reported as BQL were set equal to zero to calculate the pharmacokinetic parameters and summary statistics. The maximum plasma concentration (C_{max}) and time to maximum concentration (T_{max}) were determined directly from the concentration–time data. The data in the terminal log-linear phase were analyzed by linear regression to estimate the terminal rate constant (k) and half-life (t1/2 = 0.693/k). AUC_{0-inf} was computed as the sum of AUC_{0-t} through the last measurable concentration (C_{last}) using the linear trapezoidal rule and the terminal area.

Animal experiments

Male BALB/C nude mice, aged 30–35 days and weighing 18–22 g, were used for the animal experiments. The mice were maintained in autoclaved filter-top micro-isolator cages with autoclaved water and sterile food *ad libitum*. The cages were kept in an isolator unit that was provided with filtered air. To generate the results for Fig 5, thirty mice were subcutaneously inoculated with injections of 1×10^6 cells/nude mice. After 5 days, the tumor sizes were determined using micrometer calipers, and the nude mice with similar tumor volumes (eliminating mice with tumors that were too large or too small) were then randomly divided into three groups (10 nude mice per group): the saline tumor control group (negative control group); the oral gavage group with the oral administration of GNA002 100 mg/kg/day group; the intraperitoneal injection (i.p.) group with cisplatin (5 mg/kg/week group) or GSK126 (50 mg/kg, once per day). At the end of 4 weeks, the nude mice were sacrificed, and the tumor xenografts were excised and measured. Tumor volume (TV) was calculated using the following formula: TV (mm^3) = $d^2 \times D/2$, where d and D are the shortest and the longest diameters, respectively. The entire experimental procedure was performed in accordance with the National Institutes of Health Guide for Care and Use of Laboratory Animals (revised 1996). The experiments were performed in compliance with ethical regulations, and the protocols were approved by the institute's committee. In addition, the animals were weighed twice per week and monitored for mortality throughout the experimental period to assess treatment toxicity.

To examine tissue damage, H&E-stained tissue samples from mice receiving vehicle control were compared with tissues from mice receiving 100 mg/kg GNA002 once daily (Shangary *et al*, 2008). Histopathological analyses were performed by three independent, experienced pathologists.

Statistical analyses

Statistical analyses were performed using two-way analysis of variance (ANOVA) and unpaired two-tailed *t*-test using Prism (version 5.0) from GraphPad. $P < 0.05$ was considered significant.

Chemical preparation

Synthesis of GNA002

To a solution of GNA (26 g, 41.27 mmol, 1.0 eq) in 3 l of DCM was added HATU (14.9 g, 0.95 eq), the mixture was stirred at 0°C for 30 min, and then, a solution of 2-ethoxyethanamine (3.49 g, 0.95 eq) and TEA (4.17 g, 1.0 eq) in 500 ml of DCM was added drop-wise to the mixture at 0°C. Next, the reaction mixture was stirred at 30°C overnight. The solvent was then evaporated at 25°C by rotavapor to generate the crude GNA002, and the crude product was purified by the preparative HPLC to obtain the final GNA002 compound. Briefly, The HPLC fractions were evaporated at 25°C by rotavapor to remove most acetonitrile and then lyophilized (freeze-dried) to remove water to generate the dry power product.

Preparation of biotinylated GNA

The carboxyl group of GNA was modified by amidation with EZlink (5-biotinamido) pentylamine (Pierce) (Palempalli *et al*, 2009). Briefly, GNA (2 mg) and EZ-link (5-biotinamido) pentylamine (5 mg) were dissolved in DMSO (300 μl) and allowed to react with EDAC (1-ethyl-3-(3-dimethylaminopropyl) carbodiimide) in 100 mM MES (pH 5.5) at 37°C for 3 h. Next, the reactions were halted by extracting the products with a buffer containing ethyl acetate and MES (1:1, v/v). The extracted biotinylated GNA was then purified using the reverse-phase HPLC with a linear gradient of acetonitrile (10–100%).

Preparation for the inactive GNA008

To generate the inactive GNA derivative, GNA008, to a solution of GNA (300 mg, 0.476 mmol, 1.0 eq) in THF, 30 ml GNA008 was added an L-selectride solution in THF (0.23 ml, 0.23 mmol, 0.5 eq) drop-wise at −90°C under dry ice-acetone-liquid nitrogen. After 10 min of stirring, the reaction was quenched with 20 ml of 2 N HCl at −90°C. Then, the mixture was allowed to warm to RT and was diluted with EtOAc (20 ml). Next, the mixture was extracted with EtOAc (20 ml × 2), dried over Na_2SO_4, and evaporated by rotavapor to generate the crude inactive GNA008. Finally, the crude GNA008 product was purified by the preparative HPLC.

Expanded View for this article is available online.

Acknowledgements

We thank Prof. Ping Zhang, Dr. Rongxin Deng, and Dr. Gang Chen for critical reading of the manuscript as well as providing insightful comments for this

study. We also thank members of the W Chen and W Wei's laboratories for useful discussions. W.W. is an ACS research scholar and a LLS research scholar. This work was supported by the National Key Research and Development Program (2016YFC0902700), the National Natural Science Foundation of China (81572646, 81472515 and 91229103), project of the Shanghai Science and Technology Commission (S30206, 09431902200, 15DZ2292300 and 16431903300) and a NIH grant to W.W. (GM089763).

Author contributions

XW, ZH, SW, WW, and WC designed the study; XW, WC, JZ, MY, XW, XQ, DY, and YL performed the experiments; LW, QX, ZZ, LM, MX, and CZ reviewed the data and advised the study; XW, WW, and WC wrote the manuscript.

Conflict of interest

The authors declare that they have no conflict of interest.

References

Adams M, Cookson VJ, Higgins J, Martin HL, Tomlinson DC, Bond J, Morrison EE, Bell SM (2014) A high-throughput assay to identify modifiers of premature chromosome condensation. *J Biomol Screen* 19: 176 – 183

Arimidex TAoiCTG, Buzdar A, Howell A, Cuzick J, Wale C, Distler W, Hoctin-Boes G, Houghton J, Locker GY, Nabholtz JM (2006) Comprehensive side-effect profile of anastrozole and tamoxifen as adjuvant treatment for early-stage breast cancer: long-term safety analysis of the ATAC trial. *Lancet Oncol* 7: 633 – 643

Ashkenazy H, Erez E, Martz E, Pupko T, Ben-Tal N (2010) ConSurf 2010: calculating evolutionary conservation in sequence and structure of proteins and nucleic acids. *Nucleic Acids Res* 38: W529 – W533

Baker T, Nerle S, Pritchard J, Zhao B, Rivera VM, Garner A, Gonzalvez F (2015) Acquisition of a single EZH2 D1 domain mutation confers acquired resistance to EZH2-targeted inhibitors. *Oncotarget* 6: 32646 – 32655

Bonasio R, Tu S, Reinberg D (2010) Molecular signals of epigenetic states. *Science* 330: 612 – 616

Bonvini P, Dalla Rosa H, Vignes N, Rosolen A (2004) Ubiquitination and proteasomal degradation of nucleophosmin-anaplastic lymphoma kinase induced by 17-allylamino-demethoxygeldanamycin: role of the co-chaperone carboxyl heat shock protein 70-interacting protein. *Cancer Res* 64: 3256 – 3264

Bracken AP, Pasini D, Capra M, Prosperini E, Colli E, Helin K (2003) EZH2 is downstream of the pRB-E2F pathway, essential for proliferation and amplified in cancer. *EMBO J* 22: 5323 – 5335

Bracken AP, Helin K (2009) Polycomb group proteins: navigators of lineage pathways led astray in cancer. *Nat Rev Cancer* 9: 773 – 784

Cai Q, Sun H, Peng Y, Lu J, Nikolovska-Coleska Z, McEachern D, Liu L, Qiu S, Yang CY, Miller R, Yi H, Zhang T, Sun D, Kang S, Guo M, Leopold L, Yang D, Wang S (2011) A potent and orally active antagonist (SM-406/AT-406) of multiple inhibitor of apoptosis proteins (IAPs) in clinical development for cancer treatment. *J Med Chem* 54: 2714 – 2726

Cao R, Wang L, Wang H, Xia L, Erdjument-Bromage H, Tempst P, Jones RS, Zhang Y (2002) Role of histone H3 lysine 27 methylation in Polycomb-group silencing. *Science* 298: 1039 – 1043

Cao R, Tsukada Y, Zhang Y (2005) Role of Bmi-1 and Ring1A in H2A ubiquitylation and Hox gene silencing. *Mol Cell* 20: 845 – 854

Cao Q, Mani RS, Ateeq B, Dhanasekaran SM, Asangani IA, Prensner JR, Kim JH, Brenner JC, Jing X, Cao X, Wang R, Li Y, Dahiya A, Wang L, Pandhi M, Lonigro RJ, Wu YM, Tomlins SA, Palanisamy N, Qin Z *et al* (2011) Coordinated regulation of polycomb group complexes through microRNAs in cancer. *Cancer Cell* 20: 187 – 199

Cao J, Wan L, Hacker E, Dai X, Lenna S, Jimenez-Cervantes C, Wang Y, Leslie NR, Xu GX, Widlund HR, Ryu B, Alani RM, Dutton-Regester K, Goding CR, Hayward NK, Wei W, Cui R (2013) MC1R is a potent regulator of PTEN after UV exposure in melanocytes. *Mol Cell* 51: 409 – 422

Chang CJ, Yang JY, Xia W, Chen CT, Xie X, Chao CH, Woodward WA, Hsu JM, Hortobagyi GN, Hung MC (2011) EZH2 promotes expansion of breast tumor initiating cells through activation of RAF1-beta-catenin signaling. *Cancer Cell* 19: 86 – 100

Chopra VS, Hendrix DA, Core LJ, Tsui C, Lis JT, Levine M (2011) The polycomb group mutant esc leads to augmented levels of paused Pol II in the Drosophila embryo. *Mol Cell* 42: 837 – 844

Davalos-Salas M, Furlan-Magaril M, Gonzalez-Buendia E, Valdes-Quezada C, Ayala-Ortega E, Recillas-Targa F (2011) Gain of DNA methylation is enhanced in the absence of CTCF at the human retinoblastoma gene promoter. *BMC Cancer* 11: 232

Ezhkova E, Pasolli HA, Parker JS, Stokes N, Su IH, Hannon G, Tarakhovsky A, Fuchs E (2009) Ezh2 orchestrates gene expression for the stepwise differentiation of tissue-specific stem cells. *Cell* 136: 1122 – 1135

Ferlini C, Scambia G (2007) Assay for apoptosis using the mitochondrial probes, Rhodamine123 and 10-N-nonyl acridine orange. *Nat Protoc* 2: 3111 – 3114

Ferreira JV, Fofo H, Bejarano E, Bento CF, Ramalho JS, Girao H, Pereira P (2013) STUB1/CHIP is required for HIF1A degradation by chaperone-mediated autophagy. *Autophagy* 9: 1349 – 1366

Forbes SA, Bindal N, Bamford S, Cole C, Kok CY, Beare D, Jia M, Shepherd R, Leung K, Menzies A, Teague JW, Campbell PJ, Stratton MR, Futreal PA (2011) COSMIC: mining complete cancer genomes in the Catalogue of Somatic Mutations in Cancer. *Nucleic Acids Res* 39: D945 – D950

Galluzzi L, Senovilla L, Vitale I, Michels J, Martins I, Kepp O, Castedo M, Kroemer G (2012) Molecular mechanisms of cisplatin resistance. *Oncogene* 31: 1869 – 1883

Gibaja V, Shen F, Harari J, Korn J, Ruddy D, Saenz-Vash V, Zhai H, Rejtar T, Paris CG, Yu Z, Lira M, King D, Qi W, Keen N, Hassan AQ, Chan HM (2016) Development of secondary mutations in wild-type and mutant EZH2 alleles cooperates to confer resistance to EZH2 inhibitors. *Oncogene* 35: 558 – 566

Groll M, Schellenberg B, Bachmann AS, Archer CR, Huber R, Powell TK, Lindow S, Kaiser M, Dudler R (2008) A plant pathogen virulence factor inhibits the eukaryotic proteasome by a novel mechanism. *Nature* 452: 755 – 758

He D, Xu Q, Yan M, Zhang P, Zhou X, Zhang Z, Duan W, Zhong L, Ye D, Chen W (2009) The NF-kappa B inhibitor, celastrol, could enhance the anti-cancer effect of gambogic acid on oral squamous cell carcinoma. *BMC Cancer* 9: 343

Jones PA, Baylin SB (2007) The epigenomics of cancer. *Cell* 128: 683 – 692

Kaneko S, Li G, Son J, Xu CF, Margueron R, Neubert TA, Reinberg D (2010) Phosphorylation of the PRC2 component Ezh2 is cell cycle-regulated and up-regulates its binding to ncRNA. *Genes Dev* 24: 2615 – 2620

Kim JH, Resende R, Wennekes T, Chen HM, Bance N, Buchini S, Watts AG, Pilling P, Streltsov VA, Petric M, Liggins R, Barrett S, McKimm-Breschkin JL, Niikura M, Withers SG (2013a) Mechanism-based covalent neuraminidase inhibitors with broad-spectrum influenza antiviral activity. *Science* 340: 71 – 75

Kim W, Bird GH, Neff T, Guo G, Kerenyi MA, Walensky LD, Orkin SH (2013b) Targeted disruption of the EZH2-EED complex inhibits EZH2-dependent cancer. *Nat Chem Biol* 9: 643 – 650

Kim KH, Kim W, Howard TP, Vazquez F, Tsherniak A, Wu JN, Wang W, Haswell JR, Walensky LD, Hahn WC, Orkin SH, Roberts CW (2015) SWI/SNF-mutant cancers depend on catalytic and non-catalytic activity of EZH2. *Nat Med* 21: 1491 – 1496

Knutson SK, Wigle TJ, Warholic NM, Sneeringer CJ, Allain CJ, Klaus CR, Sacks JD, Raimondi A, Majer CR, Song J, Scott MP, Jin L, Smith JJ, Olhava EJ, Chesworth R, Moyer MP, Richon VM, Copeland RA, Keilhack H, Pollock RM *et al* (2012) A selective inhibitor of EZH2 blocks H3K27 methylation and kills mutant lymphoma cells. *Nat Chem Biol* 8: 890 – 896

Kondo Y, Shen L, Cheng AS, Ahmed S, Boumber Y, Charo C, Yamochi T, Urano T, Furukawa K, Kwabi-Addo B, Gold DL, Sekido Y, Huang TH, Issa JP (2008) Gene silencing in cancer by histone H3 lysine 27 trimethylation independent of promoter DNA methylation. *Nat Genet* 40: 741 – 750

Kronke J, Udeshi ND, Narla A, Grauman P, Hurst SN, McConkey M, Svinkina T, Heckl D, Comer E, Li X, Ciarlo C, Hartman E, Munshi N, Schenone M, Schreiber SL, Carr SA, Ebert BL (2014) Lenalidomide causes selective degradation of IKZF1 and IKZF3 in multiple myeloma cells. *Science* 343: 301 – 305

Liu CX, Yin QQ, Zhou HC, Wu YL, Pu JX, Xia L, Liu W, Huang X, Jiang T, Wu MX, He LC, Zhao YX, Wang XL, Xiao WL, Chen HZ, Zhao Q, Zhou AW, Wang LS, Sun HD, Chen GQ (2012) Adenanthin targets peroxiredoxin I and II to induce differentiation of leukemic cells. *Nat Chem Biol* 8: 486 – 493

Lu G, Middleton RE, Sun H, Naniong M, Ott CJ, Mitsiades CS, Wong KK, Bradner JE, Kaelin WG Jr (2014) The myeloma drug lenalidomide promotes the cereblon-dependent destruction of Ikaros proteins. *Science* 343: 305 – 309

Martin HL, Adams M, Higgins J, Bond J, Morrison EE, Bell SM, Warriner S, Nelson A, Tomlinson DC (2014) High-content, high-throughput screening for the identification of cytotoxic compounds based on cell morphology and cell proliferation markers. *PLoS One* 9: e88338

McCabe MT, Ott HM, Ganji G, Korenchuk S, Thompson C, Van Aller GS, Liu Y, Graves AP, Iii AD, Diaz E, Lafrance LV, Mellinger M, Duquenne C, Tian X, Kruger RG, McHugh CF, Brandt M, Miller WH, Dhanak D, Verma SK *et al* (2012) EZH2 inhibition as a therapeutic strategy for lymphoma with EZH2-activating mutations. *Nature* 492: 108 – 112

Miranda TB, Cortez CC, Yoo CB, Liang G, Abe M, Kelly TK, Marquez VE, Jones PA (2009) DZNep is a global histone methylation inhibitor that reactivates developmental genes not silenced by DNA methylation. *Mol Cancer Ther* 8: 1579 – 1588

Morris GM, Huey R, Lindstrom W, Sanner MF, Belew RK, Goodsell DS, Olson AJ (2009) AutoDock4 and AutoDockTools4: automated docking with selective receptor flexibility. *J Comput Chem* 30: 2785 – 2791

Network CGA (2012) Comprehensive molecular characterization of human colon and rectal cancer. *Nature* 487: 330 – 337

Palempalli UD, Gandhi U, Kalantari P, Vunta H, Arner RJ, Narayan V, Ravindran A, Prabhu KS (2009) Gambogic acid covalently modifies IkappaB kinase-beta subunit to mediate suppression of lipopolysaccharide-induced activation of NF-kappaB in macrophages. *Biochem J* 419: 401 – 409

Plath K, Fang J, Mlynarczyk-Evans SK, Cao R, Worringer KA, Wang H, de la Cruz CC, Otte AP, Panning B, Zhang Y (2003) Role of histone H3 lysine 27 methylation in X inactivation. *Science* 300: 131 – 135

Qi W, Chan H, Teng L, Li L, Chuai S, Zhang R, Zeng J, Li M, Fan H, Lin Y, Gu J, Ardayfio O, Zhang JH, Yan X, Fang J, Mi Y, Zhang M, Zhou T, Feng G, Chen Z *et al* (2012) Selective inhibition of Ezh2 by a small molecule inhibitor blocks tumor cells proliferation. *Proc Natl Acad Sci USA* 109: 21360 – 21365

Sahasrabuddhe AA, Chen X, Chung F, Velusamy T, Lim MS, Elenitoba-Johnson KS (2015) Oncogenic Y641 mutations in EZH2 prevent Jak2/beta-TrCP-mediated degradation. *Oncogene* 34: 445 – 454

Shangary S, Qin D, McEachern D, Liu M, Miller RS, Qiu S, Nikolovska-Coleska Z, Ding K, Wang G, Chen J, Bernard D, Zhang J, Lu Y, Gu Q, Shah RB, Pienta KJ, Ling X, Kang S, Guo M, Sun Y *et al* (2008) Temporal activation of p53 by a specific MDM2 inhibitor is selectively toxic to tumors and leads to complete tumor growth inhibition. *Proc Natl Acad Sci USA* 105: 3933 – 3938

Shen S, Zhang P, Lovchik MA, Li Y, Tang L, Chen Z, Zeng R, Ma D, Yuan J, Yu Q (2009) Cyclodepsipeptide toxin promotes the degradation of Hsp90 client proteins through chaperone-mediated autophagy. *J Cell Biol* 185: 629 – 639

Shih AH, Abdel-Wahab O, Patel JP, Levine RL (2012) The role of mutations in epigenetic regulators in myeloid malignancies. *Nat Rev Cancer* 12: 599 – 612

Sparmann A, van Lohuizen M (2006) Polycomb silencers control cell fate, development and cancer. *Nat Rev Cancer* 6: 846 – 856

Stadler ZK, Schrader KA, Vijai J, Robson ME, Offit K (2014) Cancer genomics and inherited risk. *J Clin Oncol* 32: 687 – 698

Tan J, Yang X, Zhuang L, Jiang X, Chen W, Lee PL, Karuturi RK, Tan PB, Liu ET, Yu Q (2007) Pharmacologic disruption of Polycomb-repressive complex 2-mediated gene repression selectively induces apoptosis in cancer cells. *Genes Dev* 21: 1050 – 1063

Tiedt R, Degenkolbe E, Furet P, Appleton BA, Wagner S, Schoepfer J, Buck E, Ruddy DA, Monahan JE, Jones MD, Blank J, Haasen D, Drueckes P, Wartmann M, McCarthy C, Sellers WR, Hofmann F (2011) A drug resistance screen using a selective MET inhibitor reveals a spectrum of mutations that partially overlap with activating mutations found in cancer patients. *Cancer Res* 71: 5255 – 5264

Titov DV, Gilman B, He QL, Bhat S, Low WK, Dang Y, Smeaton M, Demain AL, Miller PS, Kugel JF, Goodrich JA, Liu JO (2011) XPB, a subunit of TFIIH, is a target of the natural product triptolide. *Nat Chem Biol* 7: 182 – 188

Wei Y, Chen YH, Li LY, Lang J, Yeh SP, Shi B, Yang CC, Yang JY, Lin CY, Lai CC, Hung MC (2011) CDK1-dependent phosphorylation of EZH2 suppresses methylation of H3K27 and promotes osteogenic differentiation of human mesenchymal stem cells. *Nat Cell Biol* 13: 87 – 94

Whitesell L, Lindquist SL (2005) HSP90 and the chaperoning of cancer. *Nat Rev Cancer* 5: 761 – 772

Wu ZL, Zheng SS, Li ZM, Qiao YY, Aau MY, Yu Q (2010) Polycomb protein EZH2 regulates E2F1-dependent apoptosis through epigenetically modulating Bim expression. *Cell Death Differ* 17: 801 – 810

Wu SC, Zhang Y (2011) Cyclin-dependent kinase 1 (CDK1)-mediated phosphorylation of enhancer of zeste 2 (Ezh2) regulates its stability. *J Biol Chem* 286: 28511 – 28519

Xu T, Zhou Q, Zhou J, Huang Y, Yan Y, Li W, Wang C, Hu G, Lu Y, Chen J (2011) Carboxyl terminus of Hsp70-interacting protein (CHIP) contributes to human glioma oncogenesis. *Cancer Sci* 102: 959 – 966

Xu K, Wu ZJ, Groner AC, He HH, Cai C, Lis RT, Wu X, Stack EC, Loda M, Liu T, Xu H, Cato L, Thornton JE, Gregory RI, Morrissey C, Vessella RL, Montironi R, Magi-Galluzzi C, Kantoff PW, Balk SP *et al* (2012) EZH2 oncogenic activity in castration-resistant prostate cancer cells is Polycomb-independent. *Science* 338: 1465 – 1469

Xu B, On DM, Ma A, Parton T, Konze KD, Pattenden SG, Allison DF, Cai L, Rockowitz S, Liu S, Liu Y, Li F, Vedadi M, Frye SV, Garcia BA, Zheng D, Jin J, Wang GG (2015) Selective inhibition of EZH2 and EZH1 enzymatic activity by a small molecule suppresses MLL-rearranged leukemia. *Blood* 125: 346 – 357

Yan S, Sun X, Xiang B, Cang H, Kang X, Chen Y, Li H, Shi G, Yeh ET, Wang B, Wang X, Yi J (2010) Redox regulation of the stability of the SUMO protease SENP3 via interactions with CHIP and Hsp90. *EMBO J* 29: 3773 – 3786

Yan F, Wang M, Chen H, Su J, Wang X, Wang F, Xia L, Li Q (2011) Gambogenic acid mediated apoptosis through the mitochondrial oxidative stress and inactivation of Akt signaling pathway in human nasopharyngeal carcinoma CNE-1 cells. *Eur J Pharmacol* 652: 23 – 32

Yan J, Ng SB, Tay JL, Lin B, Koh TL, Tan J, Selvarajan V, Liu SC, Bi C, Wang S, Choo SN, Shimizu N, Huang G, Yu Q, Chng WJ (2013) EZH2 overexpression in natural killer/T-cell lymphoma confers growth advantage independently of histone methyltransferase activity. *Blood* 121: 4512 – 4520

Yu XJ, Han QB, Wen ZS, Ma L, Gao J, Zhou GB (2012) Gambogenic acid induces G1 arrest via GSK3beta-dependent cyclin D1 degradation and triggers autophagy in lung cancer cells. *Cancer Lett* 322: 185 – 194

Yu YL, Chou RH, Shyu WC, Hsieh SC, Wu CS, Chiang SY, Chang WJ, Chen JN, Tseng YJ, Lin YH, Lee W, Yeh SP, Hsu JL, Yang CC, Hung SC, Hung MC (2013) Smurf2-mediated degradation of EZH2 enhances neuron differentiation and improves functional recovery after ischaemic stroke. *EMBO Mol Med* 5: 531 – 547

Yun CH, Mengwasser KE, Toms AV, Woo MS, Greulich H, Wong KK, Meyerson M, Eck MJ (2008) The T790M mutation in EGFR kinase causes drug resistance by increasing the affinity for ATP. *Proc Natl Acad Sci USA* 105: 2070 – 2075

Zhang XW, Yan XJ, Zhou ZR, Yang FF, Wu ZY, Sun HB, Liang WX, Song AX, Lallemand-Breitenbach V, Jeanne M, Zhang QY, Yang HY, Huang QH, Zhou GB, Tong JH, Zhang Y, Wu JH, Hu HY, de The H, Chen SJ *et al* (2010) Arsenic trioxide controls the fate of the PML-RARalpha oncoprotein by directly binding PML. *Science* 328: 240 – 243

Zhen T, Wu CF, Liu P, Wu HY, Zhou GB, Lu Y, Liu JX, Liang Y, Li KK, Wang YY, Xie YY, He MM, Cao HM, Zhang WN, Chen LM, Petrie K, Chen SJ, Chen Z (2012) Targeting of AML1-ETO in t(8;21) leukemia by oridonin generates a tumor suppressor-like protein. *Sci Transl Med* 4: 127ra138

Zhou W, Ercan D, Chen L, Yun CH, Li D, Capelletti M, Cortot AB, Chirieac L, Iacob RE, Padera R, Engen JR, Wong KK, Eck MJ, Gray NS, Janne PA (2009) Novel mutant-selective EGFR kinase inhibitors against EGFR T790M. *Nature* 462: 1070 – 1074